NUMERICAL MODELING OF THE CYCLIC BEHAVIOR OF REINFORCED CONCRETE CHIMNEY SECTIONS

by

Ahmet Alperen Koç

B.S., Civil Engineering, Istanbul University, 2019

Submitted to the Institute for Graduate Studies in
Science and Engineering in partial fulfillment of
the requirements for the degree of
Master of Science

Graduate Program in Civil Engineering

Boğaziçi University

2021

To Şadihan

ACKNOWLEDGEMENTS

First of all, I would like to express my sincere gratitude to my thesis supervisor Associate Professor Sami And Kılıç for his support and guidance during my thesis study.

I would also like to show my appreciation to Prof. Cem Yalçın and Assistant Professor Gökhan Yazıcı for their comments and participation in my thesis jury.

I would like to express my special thanks of gratitude to my friend Ekrem Ekici for his support.

Finally, I would also like to extend my deepest gratitude to my family for their endless support during my whole life.

ABSTRACT

NUMERICAL MODELING OF THE CYCLIC BEHAVIOR OF REINFORCED CONCRETE CHIMNEY SECTIONS

The capability of numerical models to predict the behavior of reinforced concrete structures depends on the quality of the model, which is related to many parameters such as the definition of boundary conditions and loading, mesh quality, element formulation, material models. In this thesis, the cyclic behavior of two reinforced concrete chimney sections was numerically investigated. One of the chimney sections was oriented to be bending critical, and the other was oriented to be shear critical. Thus, major failure modes of reinforced concrete, flexural and shear, were evaluated. The performance of 4 different concrete material models in LS-DYNA, MAT_072R3 K&C, MAT_084 Winfrith, MAT_159 CSC, MAT_272 RHT, was studied. The input parameters of MAT_084, such as strain rate parameter types and values, compressive strength, tensile strength, aggregate size, and tangent modulus, were studied in detail. Other material models were used with a minimum number of inputs. The effect of material properties of the rebar was also considered. To benchmark the simulation results, the analysis results were compared with previously conducted experiments in terms of peak load, initial stiffness of load-displacement curves, the shape of hysteresis loops, pinching behavior, and stiffness degradation. The results demonstrate that the only model which shows good agreement with the experimental results is the model with the Winfrith concrete model.

ÖZET

BETONARME BACA KESİTLERİNİN TEKRARLI YÜKLEME ALTINDA DAVRANIŞININ NÜMERİK OLARAK MODELLENMESİ

Sayısal modellerin betonarme yapıların davranışını tahmin etme yeteneği, sınır koşullarının ve yüklemenin tanımı, ağ kalitesi, eleman formülasyonu, kullanılan malzeme modelleri gibi birçok parametre ile ilgili olan model kalitesine bağlıdır. Bu tezde, iki betonarme baca kesitinin tekrarlı yük altında davranışı sayısal olarak incelenmiştir. Baca kesitlerinden biri eğilme, diğeri ise kesme yönünden kritik olacak şekilde konumlandırılmıştır. Böylece, betonarmenin iki ana göçme modu olan kesme ve eğilme kırılması değerlendirilmiştir. 4 farklı beton malzeme modelinin, MAT_072R3 K&C, MAT_084 Winfrith, MAT_159 CSC, MAT_272 RHT, performansı LS-DYNA'da incelenmiştir. MAT_084'ün gerinim hızı parametreleri ve değerleri, basınç dayanımı, çekme dayanımı, agrega boyutu ve tanjant modülü gibi girdi parametreleri detaylı olarak incelenmiştir. Diğer malzeme modelleri minimum sayıda girdi parametresi ile kullanılmıştır. Donatının malzeme özelliklerinin etkisi de dikkate alınmıştır. Simülasyon sonuçlarını değerlendirmek için, analiz sonuçları, tepe yük, yük-yer değiştirme eğrilerinin başlangıç rijitliği ve şekli, çevrim sıkışması ve rijiklik azalması açısından daha önce yapılmış deneylerle karşılaştırıldı. Sonuçlar, deneysel sonuçlarla iyi uyum gösteren tek modelin Winfrith beton modeline sahip model olduğunu göstermektedir.

TABLE OF CONTENTS

ACKNOWLEDGEMENTS iv
ABSTRACT v
ÖZET vi
LIST OF FIGURES ix
LIST OF TABLES xiv
LIST OF SYMBOLS xv
LIST OF ACRONYMS/ABBREVIATIONS xvi
1. INTRODUCTION 1
1.1. Motivation 1
1.2. Literature Research 2
1.3. Objective and Scope 4
1.4. Thesis Outline 5
2. REINFORCED CONCRETE CHIMNEY SECTIONS 7
2.1. John Wilson's Experiments 7
2.2. Bending Critical Case 7
2.3. Shear Critical Case 10
3. LS-DYNA MATERIAL MODELS 14
3.1. MAT_072R3 K&C 14
3.2. MAT_084 Winfrith 15
3.3. MAT_159 CSCM 18
3.4. MAT_272 RHT 19
3.5. MAT_24 for Rebar 20
4. FINITE ELEMENT MODELING OF RC CHIMNEY SECTIONS 21
4.1. Modeling of Concrete Shell 21
4.2. Modeling of Rebars 24
4.3. Prestressing Tendons 26
4.4. Load Definition 27
4.5. Boundary Conditions 28

4.6. Material Parameters 28
4.6.1. MAT_072R3 K&C 29
4.6.2. MAT_084 Winfrith 30
4.6.3. MAT_159 CSCM 32
4.6.4. MAT_272 RHT 33
4.6.5. MAT_24 for Rebar 33
5. SIMULATION RESULTS 35
5.1. Bending Critical Case 35
5.1.1. MAT_072R3 K&C Results 35
5.1.2. MAT_084 Winfrith Results 37
5.1.3. MAT_159 CSCM Results 45
5.1.4. MAT_272 RHT Results 47
5.2. Shear Critical Case 49
5.2.1. MAT_072R3 K&C Results 49
5.2.2. MAT_084 Winfrith Results 50
5.2.3. MAT_159 CSCM Results 54
5.2.4. MAT_272 RHT Results 55
5.3. Optimum simulation parameters for Winfrith 58
6. SUMMARY AND CONCLUSIONS 62
6.1. Overview 62
6.2. Conclusions 62
6.3. Future Studies 64
REFERENCES 65
APPENDIX A: COPYRIGHTS OF FIGURES 68

LIST OF FIGURES

Figure 2.1. Bending Critical Test Set-up [9]. 9

Figure 2.2. Lateral force versus displacement for the bending critical case. . . 9

Figure 2.3. Bending Critical Case Damage [9]. 10

Figure 2.4. Shear critical deformed original cross section comparison [9]. . . . 11

Figure 2.5. Lateral force versus displacement for the shear critical case. 12

Figure 2.6. Shear Critical Case Damage. 13

Figure 3.1. The shear failure surfaces used in K&C model [13]. 15

Figure 3.2. The stress-strain curve of Winfrith model under uniaxial compression. 17

Figure 3.3. The crack opening tensile stress curve of Winfrith model. 17

Figure 3.4. CSCM yield surface in three dimensions [17]. 18

Figure 3.5. Strain softening and modulus reduction behavior of CSCM [17]. . 19

Figure 4.1. The model with 2 elements through the thickness. 23

Figure 4.2. The bending critical case model. 24

Figure 4.3. The shear critical case model. 24

Figure 4.4. The reinforcement layout of the bending critical case. 25

Figure 4.5. The reinforcement layout of the shear critical case. 26

Figure 4.6. The displacement curve of the bending critical case. 27

Figure 4.7. The displacement curve of the shear critical case. 28

Figure 5.1. The comparison of the K&C model with bending critical test result. 36

Figure 5.2. The envelope curves of the K&C model and bending critical test result. 36

Figure 5.3. The comparison of the Winfrith RATE=1 model with bending critical test result. 37

Figure 5.4. The envelope curves of the Winfrith RATE=1 model and bending critical test result. 38

Figure 5.5. The comparison of the Winfrith models with RATE=1 and RATE=2. 39

Figure 5.6. The envelope curves of the Winfrith RATE=2 model and bending critical test result. 39

Figure 5.7. The comparison of the Winfrith models with with RATE=1 and RATE=0. 40

Figure 5.8. The envelope curves of the Winfrith RATE=0 model and bending critical test result. 40

Figure 5.9. The comparison of the Winfrith models with different fracture energy. 41

Figure 5.10. The comparison of the Winfrith models with different maximum aggregate sizes. 42

Figure 5.11. The comparison of the Winfrith models with different concrete tensile strengths. 42

Figure 5.12. The comparison of the Winfrith models with different elastic moduli. 43

Figure 5.13. The comparison of the Winfrith models with different f_c. 44

Figure 5.14. The comparison of the models with different tangent moduli. . . . 45

Figure 5.15. The comparison of the models with different yielding stresses. . . . 45

Figure 5.16. The comparison of the CSCM with bending critical test result. . . 46

Figure 5.17. The envelope curves of the CSCM and bending critical test result. 46

Figure 5.18. The comparison of the RHT model with bending critical test result. 47

Figure 5.19. The envelope curves of the RHT model and bending critical test result. 48

Figure 5.20. The failed RHT model for the bending critical case. 48

Figure 5.21. The comparison of the K&C model with shear critical test result. . 49

Figure 5.22. The envelope curves of the K&C model and shear critical test result. 50

Figure 5.23. The comparison of the Winfrith RATE=1 model with shear critical test result. 51

Figure 5.24. The envelope curves of the Winfrith RATE=1 model and shear critical test result. 51

Figure 5.25. The comparison of the Winfrith models with RATE=1 and RATE=2 for the shear critical case. 52

Figure 5.26. The envelope curves of the Winfrith RATE=2 model and shear critical test result. 53

Figure 5.27. The comparison of the Winfrith models with RATE=1 and RATE=0 for the shear critical case. 53

Figure 5.28. The envelope curves of the Winfrith RATE=0 model and shear critical test result. 54

Figure 5.29. The comparison of the CSCM with shear critical test result. . . . 55

Figure 5.30. The envelope curves of the CSCM and shear critical test result. . . 55

Figure 5.31. The comparison of the RHT model with shear critical test result. . 56

Figure 5.32. The envelope curves of the RHT model and shear critical test result. 57

Figure 5.33. The failed RHT model for the shear critical case. 57

Figure 5.34. The comparison of the Winfrith model with RATE=0 and RATE=1 combined with reduced elastic modulus for the bending critical case. 58

Figure 5.35. The comparison of the Winfrith model with RATE=0 and RATE=1 combined with reduced elastic modulus for the shear critical case. 59

Figure 5.36. The predicted cracks for the bending critical case. 59

Figure 5.37. The predicted cracks for the shear critical case. 60

Figure A.1. Copyrights of Figure 2.1, 2.3, and 2.4. 68

Figure A.2. Copyrights of Figure 3.1 page 1. 69

Figure A.3. Copyrights of Figure 3.1 page 2. 70

LIST OF TABLES

Table 2.1. Summary of the bending critical pipe properties. 8

Table 2.2. Summary of the shear critical pipe properties. 12

Table 4.1. The list of hourglass control types in LS-DYNA. 22

Table 4.2. The consistent units used. 29

Table 4.3. The input parameters of K&C model. 30

Table 4.4. The input parameters of Winfrith model. 31

Table 4.5. The alternative input parameters of Winfrith model. 32

Table 4.6. The input parameters of CSCM model. 32

Table 4.7. The input parameters of RHT model. 33

Table 4.8. All input parameters of MAT_24 model. 34

Table 5.1. The summary of sensitivity analysis of Winfrith. 61

LIST OF SYMBOLS

f_{cm}	Mean compressive strength
f'_c	Unconfined compressive stress
f'_t	Uniaxial tensile strength
G_F	Fracture energy
I_1	First stress invariant
I_2	Second stress invariant
I_3	Third stress invariant
J_2	Second deviatoric stress invariant
J_3	Third deviatoric stress invariant
w	Crack width at which crack-normal tensile stress goes to zero
θ	Lode angle
σ_1	First principal stress
σ_2	Second principal stress
σ_3	Third principal stress

LIST OF ACRONYMS/ABBREVIATIONS

3D	Three Dimensional
ACI	American Concrete Institute
CDPM	Concrete Damage Plasticity Model
CEB	Comité Européen du Béton
CICIND	Comité International Des Construction Industrielles
CSCM	Continuous Surface Cap Model
FE	Finite Element
FIP	Fédération Internationale de la Précontrainte
K&C	Karagozian and Case
RC	Reinforced Concrete

1. INTRODUCTION

1.1. Motivation

Experimental studies are still the main way to learn more about the behavior of reinforced concrete structures, but it is hard to conduct full-scale or scaled tests for every case due to time and budget constraints. Especially for large and complex structures such as chimneys, experimental studies are expensive. Therefore, the numerical modeling of reinforced concrete structures is an active research area. The validated numerical models can be great tools for researchers and engineers. With the help of these models, engineers can design safe structures and researchers can carry out parametric studies to learn more about structures.

The complex nature of the three-dimensional stress-strain behavior of the concrete makes it difficult to model. Additionally, complicated effects of shear-flexure interaction, strain rate, aggregate interlock, bond-slip behavior of reinforcement, cracking of the concrete make the modeling of RC structures even more problematic. Nonlinear analysis of reinforced concrete structures is dated back to the 1960s [1]. There are various material models for concrete and reinforcement steel [1]. Some of these material models are implemented in commercial finite element software such as LS-DYNA which has several material models for concrete. Numerous validation studies can be found in the literature for these material models [2] but the vast majority of them were tested against blast or impact type of loading which is different than seismic loading in terms of duration and strain rate. In literature, there is a limited validation study about the seismic performance of LS-DYNA concrete material models [3]. The validity of these models is of great importance to be able to make the numerical models accurate. The sophisticated concrete models in LS-DYNA sometimes require tens of input parameters because all of these material models cannot generate the remaining parameters automatically with a limited number of input parameters such as compressive strength and density of the concrete. Even if the material model can work with a few inputs, it

may not capture the behavior of the specific type of concrete, because these automatic parameter generator algorithms are calibrated to certain types of concrete. For that reason, the determination of model parameters for different types of concrete such as fiber-reinforced concrete can be found in the literature [4].

The calibration and sensitivity analysis of these material models are of great interest to researchers and engineers. There is a huge amount of study in this area but the studies concerning the seismic application of these material models are limited in the literature. Understanding the strength and weaknesses and limitations of these material models to simulate the seismic response of reinforced concrete structures is important especially for seismically active regions.

1.2. Literature Research

Coleman [3] studied four LS-DYNA concrete material models, MAT_072R3 K&C, MAT_084 Winfrith, MAT_159 CSCM, and MAT_272 RHT, in terms of their performance in seismic applications. In the first part of the study, he conducted single-element monotonic compression analyses for each material model to evaluate the effect of element size, element formulation, hourglass formulation, and strain rate. Unconfined uniaxial tension, biaxial compression-tension, cyclic compression, and cyclic compression-tension simulations were carried out on single elements to assess the ability of material models to reproduce the seismic response of reinforced concrete. After single-element analyses, two multi-element numerical models were created for each material model to reproduce the experimental results. The first one was a cyclic compression of a cylinder specimen and the second one is a cyclic bending test of a cantilever reinforced concrete beam. The strength and weaknesses of each material model were discussed concerning the capability of models to capture the shear and cyclic behavior of concrete and the sensitivity to mesh size, element, and hourglass formulation after single-element simulations. Some recommendations were made for each material as a conclusion. Winfrith model performed better compared to the other three concrete models but it was concluded that none of these material models were appropriate to

simulate time history analysis due to their overprediction of energy dissipation during the analysis.

Asgarpoor et al. [5] investigated the performance of five LS-DYNA concrete models, MAT_072R3, MAT_084, MAT_159 MAT_272, and MAT_273, under cyclic loading. MAT_ADD_EROSION with minimum principal strain option was used to model the crushing of concrete. One rectangular beam, one T-shaped beam, two columns, and five shear walls were modeled in LS-DYNA. To able to investigate different structural responses of reinforced concrete elements, shear walls that have different reinforcement and aspect ratios, with and without boundary elements and short and slender columns were selected. The initial stiffness, peak strength, drift at the onset of strength loss values were compared with experimental results. The predicted and measured lateral displacement-lateral force curves were contrasted. The observed and predicted damage and failure modes were examined. The pinching of reinforced concrete elements was only predicted by MAT_084 (Winfrith) concrete model. The strengths and weaknesses of material models were discussed.

The in-plane seismic behavior of lightly reinforced and low aspect ratio reinforced concrete shear walls were numerically investigated by Epackachi and Whittaker [6]. The experimental data of twenty-two RC walls with a different aspect and reinforcement ratios, axial load, and material properties were used for the validation of the numerical model. Winfrith concrete model was used in simulations. A numerical technique was suggested to model restrained shrinkage and early cracking which affect the initial stiffness of the wall. Strength loss of concrete after the peak strength was implemented by MAT_ADD_EROSION. The numerical results demonstrated reasonable estimations of the peak strength, post-peak strength degradation, and pinching.

Bohara et. al. [7] used a non-ductile reinforced concrete column to investigate the concrete material models, Winfrith, K&C, and Continuous Surface Cap, with minimum input parameters under lateral cyclic loading. Predicted and measured drift-lateral load values were compared and fringes of maximum principal strain were demonstrated. CSCM concrete model predicted peak load and drift ratios with good accuracy. The

energy dissipation was overpredicted by the simulations especially after yielding of reinforcements.

Winkelbauer [8] evaluated the performance of five concrete material models, MAT_072R3, MAT_084, MAT_159, MAT_272, and MAT_273, to simulate unreinforced concrete. Single-element and multi-element simulations were conducted to assess the performance of the models under tension, compression, and shear. One experimental study was selected from the literature and the results were reproduced numerically and the measured and predicted results were compared. The K&C and CSCM performed relatively better in the single-element and the comparison simulations. Additionally, laboratory tests on the cylinder, beam, and dogbone specimens were carried out to examine the capability of the two of the material models, K&C and CSCM, to simulate the behavior of plain concrete under tension, compression, and flexure loadings.

The single-element and structural element test simulations can provide useful insight into the material models. However, the numerical modeling of non-traditional structures such as chimneys needs special attention to produce accurate results.

1.3. Objective and Scope

The objective of this study is to validate the Winfrith concrete model to simulate the cyclic behavior of reinforced concrete chimneys and to compare the performance of the Winfrith model with three commonly used LS-DYNA concrete models with minimum input parameters. The sensitivity analysis was carried out for the input parameters of the Winfrith model to understand the model's behavior.

Within the scope of this work, two reinforced concrete chimney sections studied experimentally by Wilson in [9] were simulated under cyclic loading in LS-DYNA. One of the chimney sections was oriented to be bending critical, and the other was oriented to be shear critical to simulate two major failure modes of reinforced concrete. Four commonly used concrete models, K&C, Winfrith, CSC, and RHT, were tested but the

K&C, CSC, and RHT models were utilized with minimum input parameters. The performance of the numerical models was assessed by comparing the predicted and measured responses such as the peak load, initial stiffness, and stiffness degradation. MAT_024 Piecewise Linear Plasticity model was used for the reinforcing rebars and the effect of the tangent, and young modulus of the reinforcement was investigated.

1.4. Thesis Outline

This thesis consists of 6 chapters. Chapter 1 is the introductory chapter which provides the motivation of the study, the literature review, and the objective and scope.

In Chapter 2, information about the experimental studies which were used for the validation was given. The experimental setup details, material properties for the two reinforced concrete chimney sections modeled, and the results of the studies were also provided.

Chapter 3 introduces LS-DYNA material models used in the study for the concrete and the rebar. The theoretical background informations about the material models were given.

Chapter 4 gives finite element modeling details of the study. The mesh geometry and the element types that were used to model the concrete and rebars were discussed. The modeling of the prestressing tendons used for axial loading and the application of loading were explained. The material input parameters that define the properties of the material models for each material model were examined and the used parameters were listed.

In Chapter 5, the simulation results for two reinforced concrete chimney sections were given. The comparison of numerical results and the experimental results were made.

Chapter 6 provides the summary of the thesis and conclusions. It also contains recommendations for future studies.

2. REINFORCED CONCRETE CHIMNEY SECTIONS

2.1. John Wilson's Experiments

John Wilson conducted experiments to investigate the cyclic behavior of reinforced concrete chimneys. He first carried out tests on four circular hollow reinforced concrete test units without openings [10]. Then, a reinforced concrete pipe with openings was tested under cyclic loading in [11]. The pipe was oriented such that openings were on the faces experienced maximum bending strains. This test henceforth will be called the bending critical case. To consider the shear failure, another reinforced concrete pipe was tested such that the openings were orientated to be shear critical [12]. The last test hereafter will be called the shear critical case. In the following two sections, experimental test set-ups and test results for the bending and shear critical tests will be discussed in detail.

2.2. Bending Critical Case

The test arrangement can be seen in Figure 2.1 [9]. The RC pipe with a thickness of 40 mm was supported by a 320 mm thick reinforced concrete block and this support was fixed to the steel anchor block. A commercial pipe with a 2.2 m length was used because a 40-mm thick cross-section is not appropriate to build with conventional construction techniques. To increase the shear span to member diameter ratio, a steel tube was connected to the reinforced concrete pipe with twelve steel straps, and a total of 4600 mm length hybrid pipe was achieved.

Two prestressing cables were used to apply an axial load of 226 kN which creates 1.55 MPa axial stress to simulate gravity loading. The pipe has two 600 mm wide openings which are the largest permissible openings by CICIND and ACI 307 design codes. The openings are facing each other and are located 300 mm from the fixed end. Table 2.1 summarizes the properties of the RC pipe tested for the bending critical case.

Table 2.1. Summary of the bending critical pipe properties.

Properties of the pipe	**Value**
Openings	2 600 × 600 mm
Length	4600 mm
Outer Diameter	1194 mm
Thickness	40 mm
D/t	30
Axial Stress	1.55 MPa
f_c	40 MPa
Reinforcement ratio	0.53%
Rebar stress f_y	530 MPa
Rebar stress $f_{3\%}$	560 MPa
Rebar stress f_u	590 MPa

Deformed rebars with a diameter of 5.8 mm and 125 mm spacing were used as longitudinal reinforcements and were centrally placed. The 4.8 mm diameter rebars were placed in a helix at 80 mm centers for the hoop steel. Three additional rebars were added to each side of the openings within a 100 mm distance per the design code recommendations. The reinforcements were heated to increase their ductility. The cyclic lateral load was exerted by applying displacement-controlled loading using a hydraulic actuator.

The bending critical pipe showed limited ductility and reached a drift ratio of 1.5% which corresponds to 67 mm displacement after five cycles. The lateral force versus displacement plot can be seen in Figure 2.2. The pipe failed during the sixth cycle due to the buckling and fracture of reinforcement bars near the opening. The damage adjacent to the opening is demonstrated in Figure 2.3 [9]. Serious distortion of the cross-section in the vicinity of the openings was noticed.

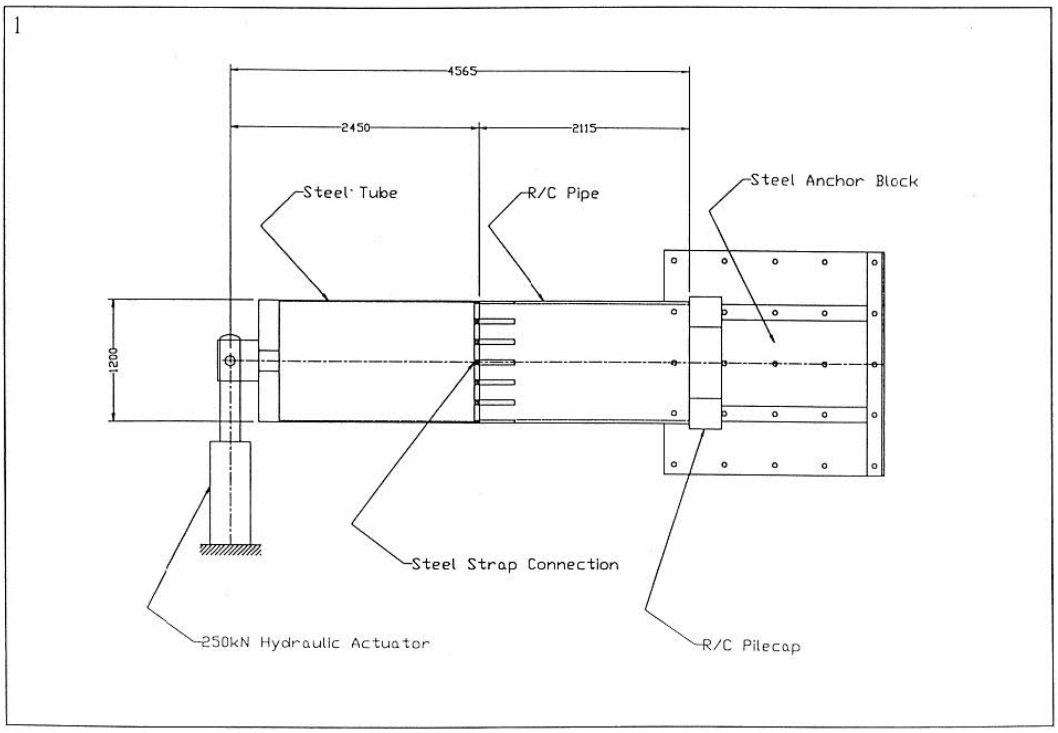

Figure 2.1. Bending Critical Test Set-up [9].

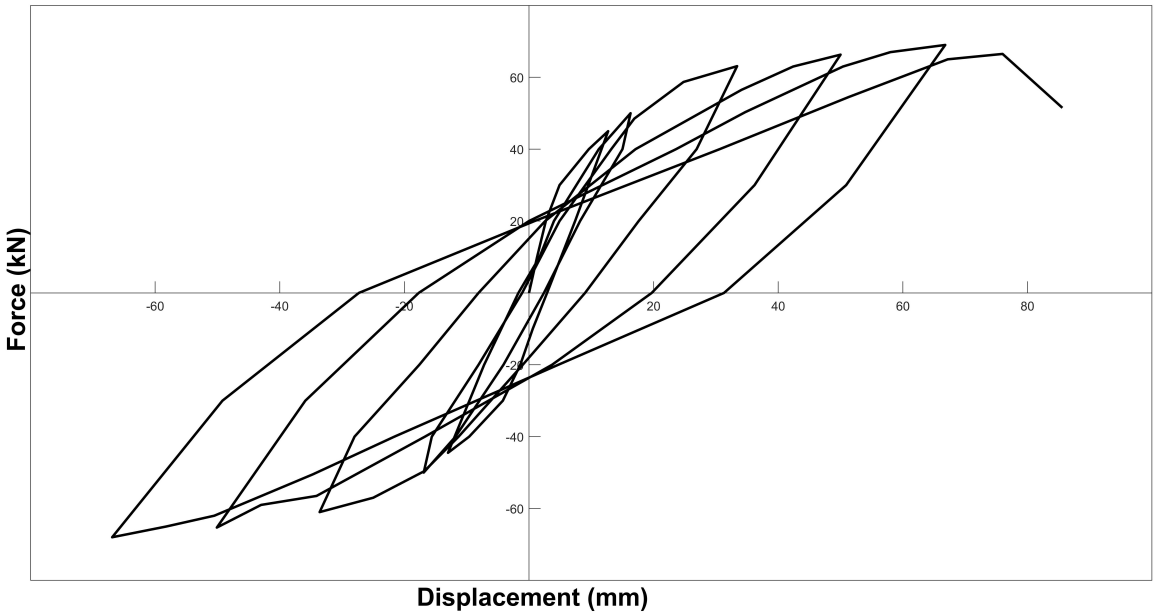

Figure 2.2. Lateral force versus displacement for the bending critical case.



Figure 2.3. Bending Critical Case Damage [9].

2.3. Shear Critical Case

A similar test set-up to the bending critical case was configured for the shear critical case. An equivalent hybrid pipe was used. The pipe failed due to local failure at the fixed end but the remainder of the pipe experienced only minor crackings. Instead

of a new specimen, the pipe was retrofitted by inserting the 300 mm end portion of the pipe into the anchor block and prestressing with bolts. As a result of the encasement of the pipe, the openings were next to the fixed base and the total length of the pipe was reduced to 4345 mm. Two openings have a dimension of 600 mm by 800 mm.

The heat-treated deformed rebars were used with the same dimensions and arrangement of the bending critical case including the extra rebars around the openings. Table 2.2 shows the properties of the reinforced concrete pipe tested for the shear critical case.

To measure the distortions, a 3D photogrammetry technique was implemented. The deformed-original cross-section comparison can be seen in Figure 2.4 [9]. The shear critical pipe demonstrated also limited ductility with a drift ratio of 1.8% (after 8 cycles) which corresponds to 78 mm displacement. The lateral force versus displacement curve was shown in Figure 2.5. The pipe was deemed to fail at a tip displacement of 87 mm corresponds to a drift ratio of 2%. The failure occurred due to the buckling of the concrete shell under compression adjacent to the fixed end. In Figure 2.6, the damage can be seen.(J.L. Wilson, personal communication, August 25, 2009)

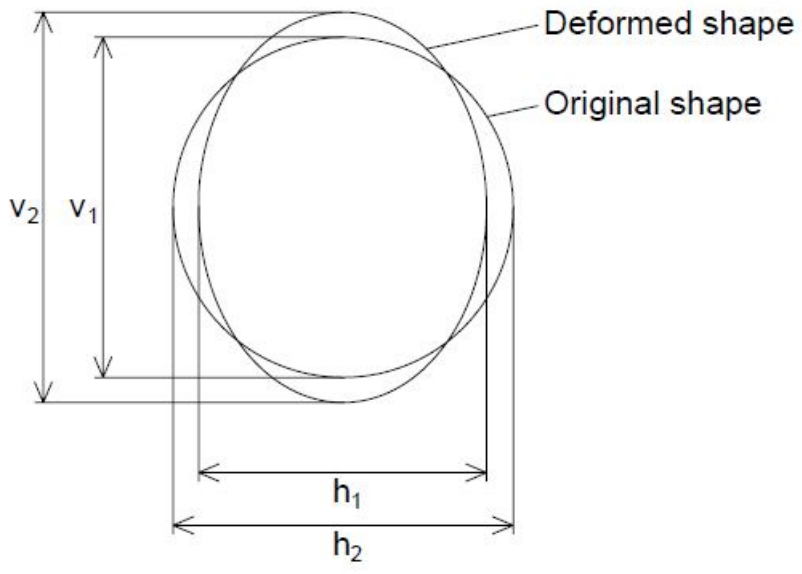

Figure 2.4. Shear critical deformed original cross section comparison [9].

Table 2.2. Summary of the shear critical pipe properties.

Properties of the pipe	**Value**
Openings	2 600 × 800 mm
Length	4345 mm
Outer Diameter	1194 mm
Thickness	40 mm
D/t	30
Axial Stress	1.55 MPa
f_c	40 MPa
Reinforcement ratio	0.53%
Rebar stress f_y	530 MPa
Rebar stress $f_{3\%}$	560 MPa
Rebar stress f_u	590 MPa

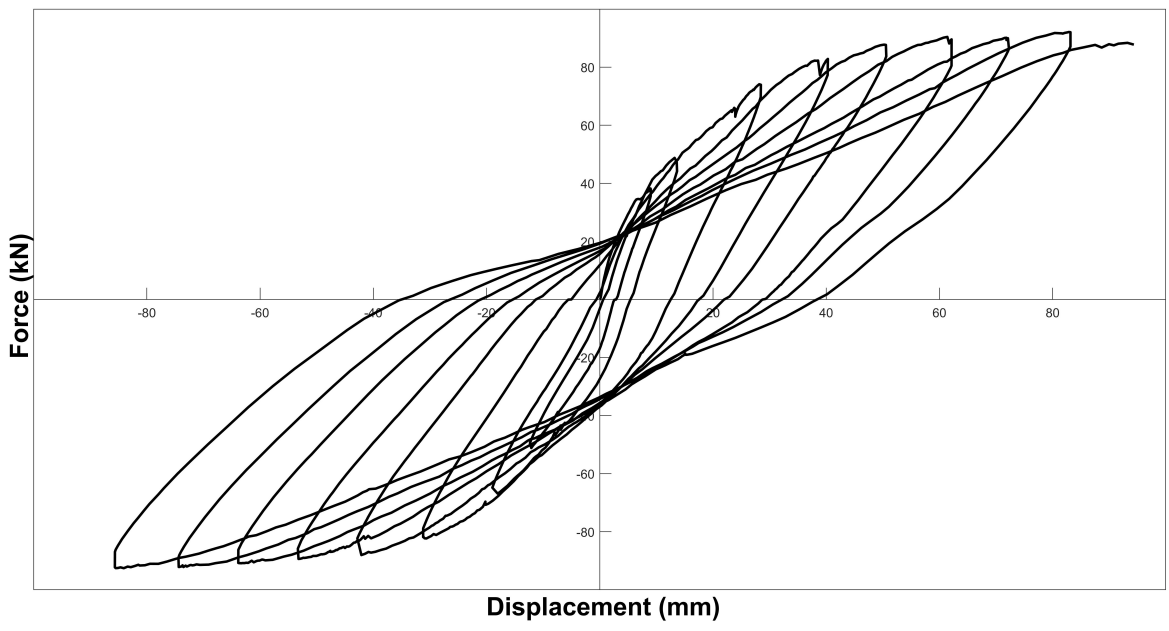

Figure 2.5. Lateral force versus displacement for the shear critical case.

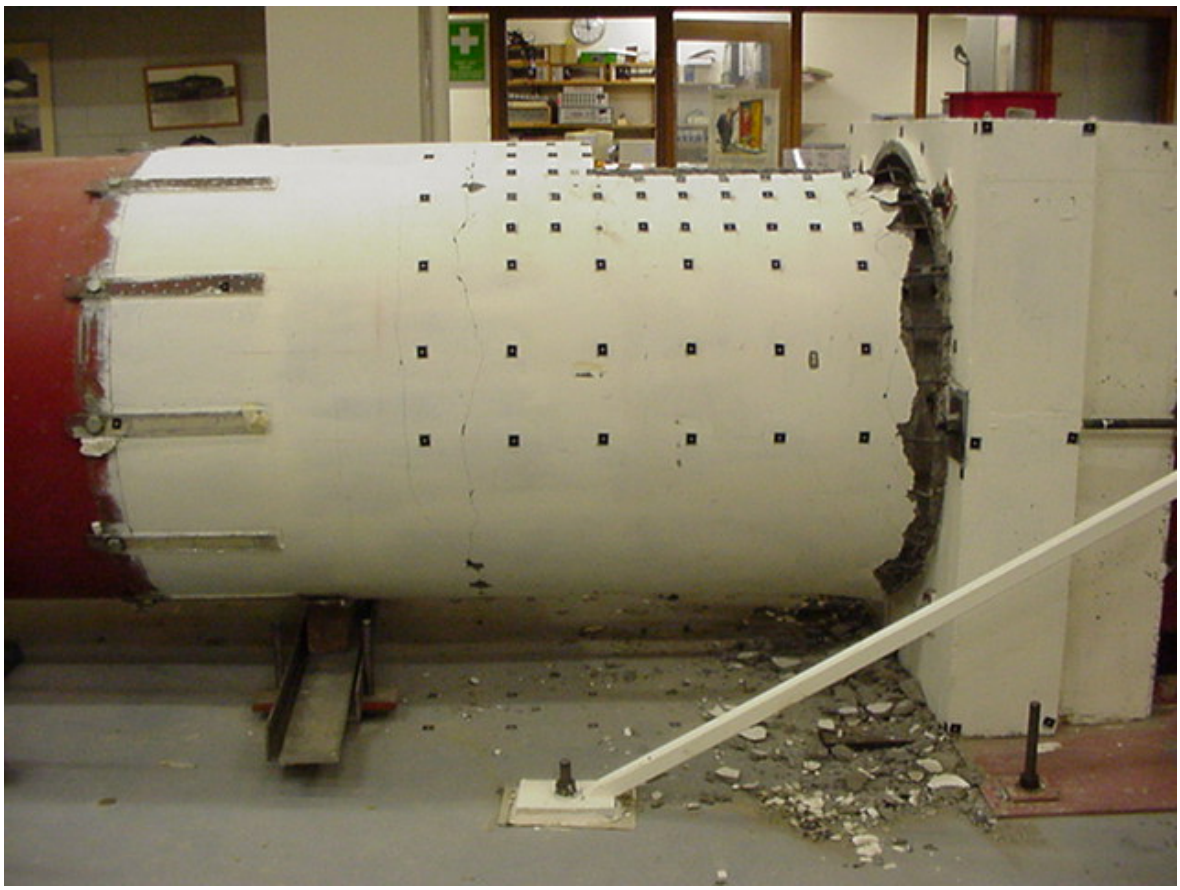

Figure 2.6. Shear Critical Case Damage.

3. LS-DYNA MATERIAL MODELS

Before carrying out the validation of the numerical models, it is important to understand the theory of the material models used in the study because each material model was developed based on a different theory that builds upon different assumptions. In the following section, four selected concrete material models and one model for the reinforcing rebars will be discussed.

3.1. MAT_072R3 K&C

MAT_072R3 is the third and last release of the concrete damage model which is also known as the Karagozian and Case concrete model and is available from v971 of LS-DYNA. The first release of the model was developed by Malvar et al [13]. A series of modifications were made on the material model 16 of DYNA3D to create a new material model. The second release which includes shear dilation was released in 1996 [14]. The last release of the model includes the automatic input parameter generator which requires only the unconfined compressive strength of the concrete.

MAT_072 Release III is a three-invariant model that utilizes three shear failure surfaces based on Willam and Warnke criterion. A total of eight parameters are required to define these surfaces. In Figure 3.1, the shear surfaces are depicted [13]. The equations defining the maximum failure surface, the residual failure surface, and the yield failure surface are given respectively as

$$\Delta\sigma_m = a_0 + \frac{p}{a_1 + a_2 p}\,, \tag{3.1}$$

$$\Delta\sigma_r = \frac{p}{a_{1f} + a_{2f} p}\,, \tag{3.2}$$

$$\Delta\sigma_y = a_{0y} + \frac{p}{a_{1y} + a_{2y} p}\,. \tag{3.3}$$

a_{0y}, a_{1y}, a_{2y}, a_0, a_1, a_2, a_{1f}, and a_{2f} are parameters calibrated from the test data and p

is the pressure which is equal to negative of $I_1/3$ where I_1 is the first stress invariant defined as

$$I_1 = \sigma_1 + \sigma_2 + \sigma_3. \tag{3.4}$$

The model includes strain rates and defines the pressure-volumetric strain with an equation of state.

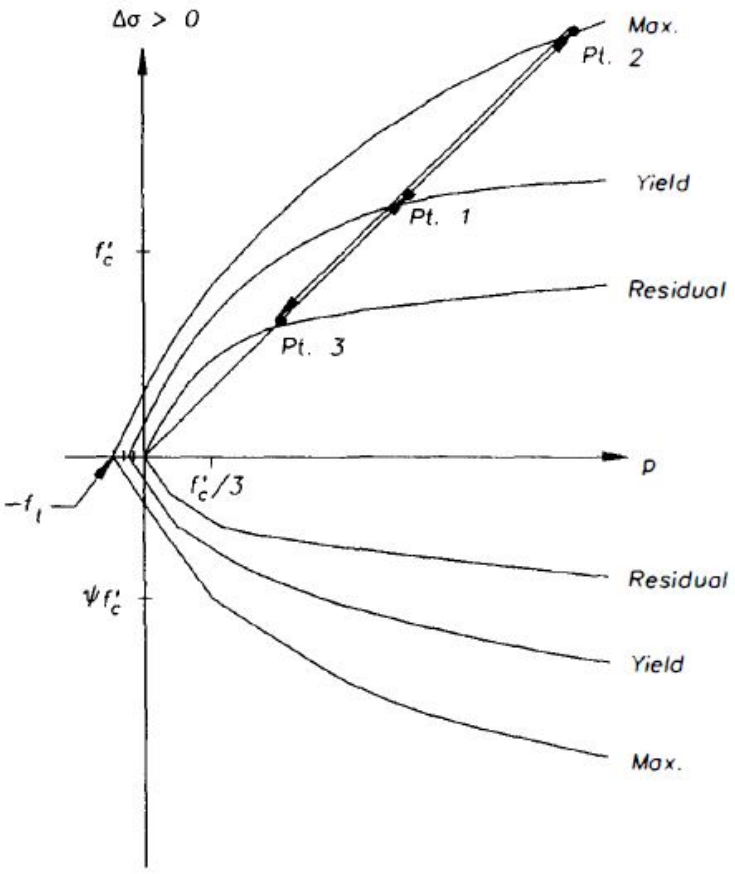

Figure 3.1. The shear failure surfaces used in K&C model [13].

3.2. MAT_084 Winfrith

The Winfrith concrete model was developed to predict the response of RC structures to impact loadings in the 1980s [15]. It is a smeared crack, i.e, pseudo crack model

and its plasticity portion is based on a four-parameter model proposed by Ottosen [16]. The failure criterion is defined as

$$F\left(I_1, J_2, \cos 3\theta\right) = a\frac{J_2}{\left(f_c'\right)^2} + \lambda\frac{\sqrt{J_2}}{f_c'} + b\frac{I_1}{f_c'} - 1, \tag{3.5}$$

$$\lambda = \begin{cases} k_1 \cos\left[\frac{1}{3}\cos^{-1}\left(k_2\cos(3\theta)\right)\right] & \cos(3\theta) \geq 0 \\ k_1 \cos\left[\frac{\pi}{3} - \frac{1}{3}\cos^{-1}\left(-k_2\cos(3\theta)\right)\right] & \cos(3\theta) \leq 0 \end{cases} \tag{3.6}$$

$$\cos 3\theta = \frac{3\sqrt{3}}{2}\frac{J_3}{J_2^{1.5}} \tag{3.7}$$

where I_1 is the first stress invariant, J_2 is the second deviatoric stress invariant, f'$_c$ is the unconfined compressive stress. a, b, k_1, and k_2 are parameters and are determined by uniaxial compression, biaxial compression, triaxial compression, and uniaxial tension test.

Winfrith concrete model behaves in an elastic perfectly plastic manner under uniaxial compression. On the other hand, the stress-strain relationship under uniaxial tension is linear up to cracking. After the cracking, the crack normal stress decreases linearly as a function of crack width. The stress-strain curve under uniaxial compression and the crack opening tensile stress curve can be seen in Figure 3.2 and Figure 3.3, respectively. The model can form 3 orthogonal cracks which are created in the perpendicular direction to the principal tensile stresses in a single brick element. In addition, the Winfrith concrete model takes into account the aggregate interlock which is the shear force transfer between two opposing crack surfaces. The transferred shear stress on a crack element is calculated by multiplying the shear stress with a coefficient which is a function of crack width and the aggregate diameter.

Additionally, the model has an option to model the rebars. The option requires the yield strength, Young and hardening modulus, and ultimate elongation of the rebars. To place the reinforcement, an extra keycard that locates the reinforcements is required.

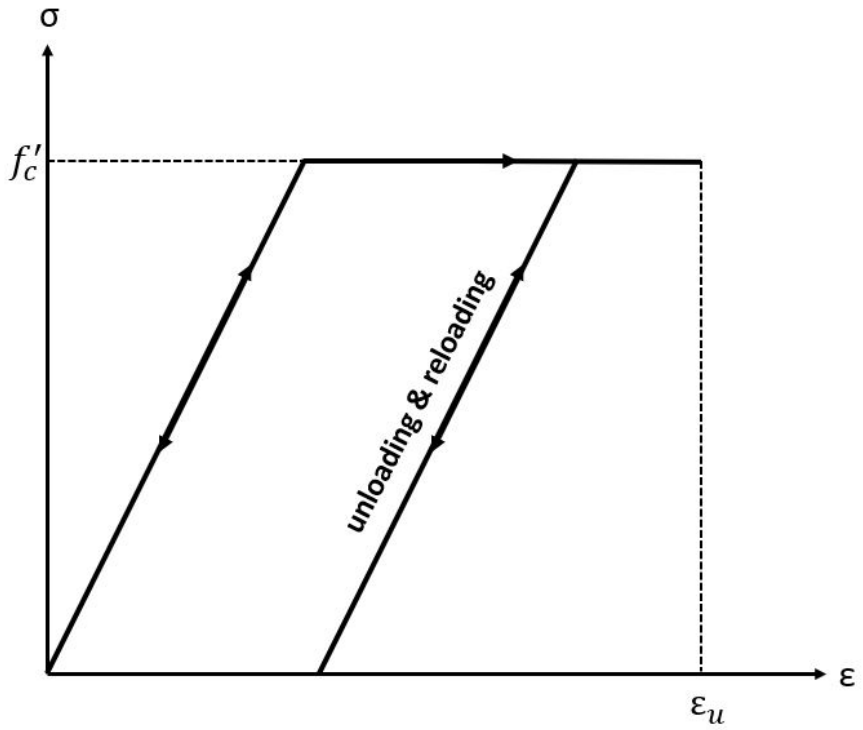

Figure 3.2. The stress-strain curve of Winfrith model under uniaxial compression.

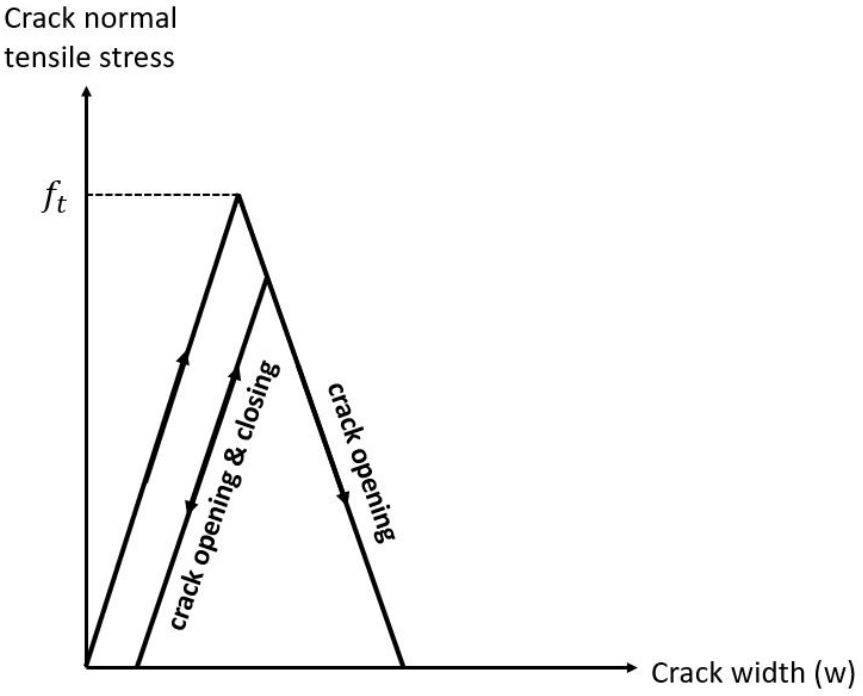

Figure 3.3. The crack opening tensile stress curve of Winfrith model.

3.3. MAT_159 CSCM

Continuous Surface Cap Model (MAT_159) was developed for the National Cooperative Highway Research Program to simulate the concrete used in road safety structures under dynamic loadings [17]. The model was implemented into the 971 version of LS-DYNA. MAT_159 keycard has two options which are MAT_CSCM and MAT_CSCM_CONCRETE. In MAT_CSCM, the user should provide all material properties such as hardening and softening parameters. On the other hand, the second option can use default parameters for the normal concrete. The model provides the default parameters based on the unconfined compression strength, the aggregate size, and the units [18]. The default parameters were obtained by fitting the data of normal concretes which have unconfined compressive strength between 20 and 58 MPa.

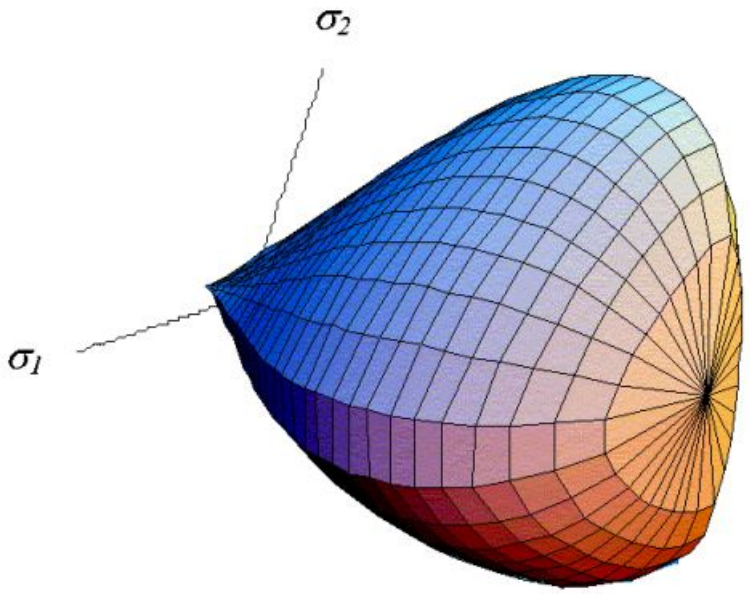

Figure 3.4. CSCM yield surface in three dimensions [17].

The model combines the shear failure surface with the cap surface smoothly and continuously. The yield surface of the concrete model is illustrated in Figure 3.4 [17]. Originally, the smooth cap model is a two-invariant model but it was extended to a three-invariant formulation. The yield surface is a function of the first stress invariant,

the second deviatoric stress invariant, and the third deviatoric stress invariant.

The CSCM behaves perfectly plastic under uniaxial tension, unconfined compression, three-axial tension, and three-axial compression without damage formulation. The damage formulation can model the strain-softening after the peak load. It is also capable of modeling the modulus reduction during cyclic loading unloading. The strain softening and modulus reduction behavior of the model is shown in Figure 3.5.

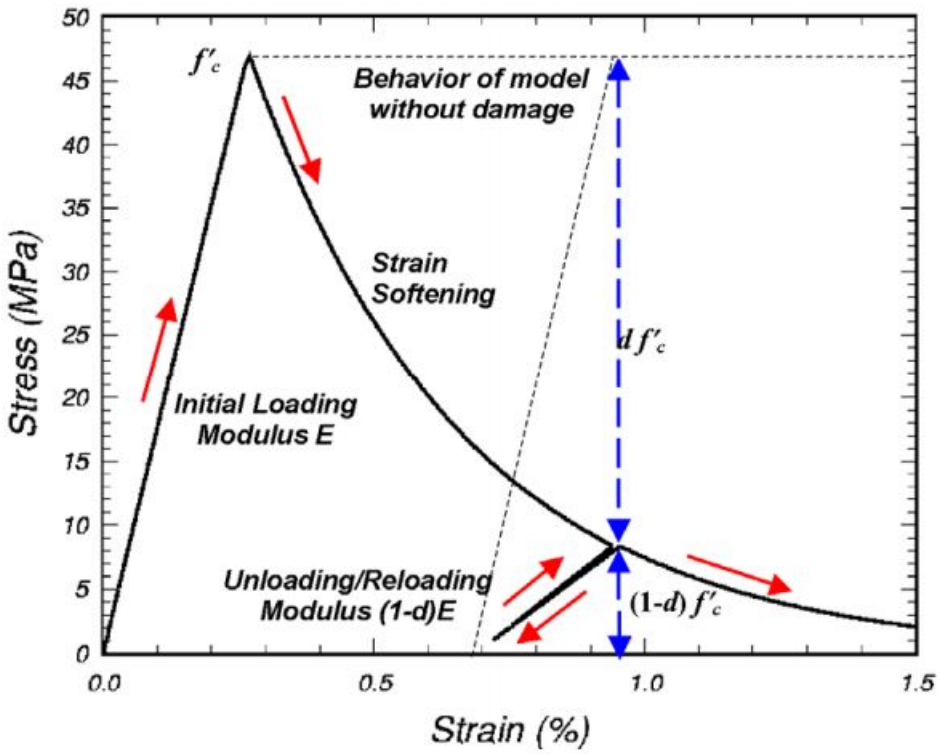

Figure 3.5. Strain softening and modulus reduction behavior of CSCM [17].

3.4. MAT_272 RHT

MAT_272 RHT was developed by enhancing the Johnson–Holmquist damage model [19]. It was developed for analyzing rocks under impulsive and impact loadings [8].

The RHT model considers three pressure-dependent surfaces, namely an elastic

limit surface, a failure surface, and a residual surface. The Mie-Gruneisen equation of state was used to define the pressure.

The input of the unconfined compressive strength of the concrete is enough to generate the remaining parameters. The default compressive strength of the model is 35 MPa and the model interpolates between 35 MPa and 140 MPa to generate other material parameters [8]. The model is strain-rate sensitive as the other three models.

3.5. MAT_24 for Rebar

MAT_024 is an elastoplastic material model that can define arbitrary stress-strain and strain rate dependency relationships [20]. Alternatively, a bilinear stress-strain curve can be defined. The model uses von Mises, i.e., J_2 based plasticity model for the yield function. MAT_024 can consider failure based on the effective plastic strain or user-defined failure subroutine. It has also automatic element deletion controlled by minimum time-step.

4. FINITE ELEMENT MODELING OF RC CHIMNEY SECTIONS

The 3D finite element models of the RC pipes were created in LS-DYNA that has both implicit and explicit solvers [21]. The explicit solver uses the central difference scheme to evaluate the equation of motion in each step. The drawback of explicit solvers is that the time step should be small enough to satisfy the Courant–Friedrichs–Lew condition which is a convergence criterion. For this reason, each simulation takes about 20 hours on a computer with an i7 eight-core processor.

In the following section, the details about the modeling of the reinforced concrete chimney sections will be given. The element and hourglass formulations, the definition of the loading, the element types, the boundary conditions, and the material models' parameters will be discussed in detail.

4.1. Modeling of Concrete Shell

8-node hexahedral solid elements, i.e., brick elements were used to model the concrete shell. There are several element formulations for solid elements in LS-DYNA [20]. Element formulation 1 which is the default element formulation was used in this study. This element formulation creates reduced integration elements that use one-point Gauss quadrature for numerical integration. Stress is constant inside these elements. The advantage of reduced-integration elements is that they are more efficient than fully integrated elements in terms of computation time. Additionally, reduced integrated elements eliminate the shear locking defect of fully integrated elements. But reduced integration elements are prone to hourglass modes and need hourglass stabilization.

Hourglass modes are zero-energy modes that have no physical meaning. There are nine hourglass control types for solid elements in LS-DYNA [20]. These control

Table 4.1. The list of hourglass control types in LS-DYNA.

IQH No	Hourglass stabilization form
1	Standard LS-DYNA viscous
2	Flanagan-Belytschko viscous
3	Flanagan-Belytschko viscous with exact volume integration
4	Flanagan-Belytschko stiffness
5	Flanagan-Belytschko stiffness with exact volume integration
6	Belytschko-Binderman
7	Belytschko-Binderman with linear total strain
9	Puso
10	Cosserat Point Element

types are listed in Table 4.1. Flanagan-Belytschko stiffness form with exact volume integration (type 5) was used throughout this study. Coleman showed that K&C and Winfrith were not affected by element formulation and hourglass control. However, the responses of models with CSCM and RHT were different for different element formulations and hourglass stabilization forms. Element formulation 1 with a stiffness type hourglass control was performed well with all material models except the RHT models where element formulation 1 with a viscous type of hourglass stabilization was recommended. But it was also indicated that viscous type of hourglass controls are best used in high-velocity problems. This limitation makes the use of the RHT model problematic for low-velocity seismic problems. Detailed information about the effects of hourglass control types can be found in [3].

The concrete shell of the shear and bending critical cases were meshed using 20 mm thick brick elements through the thickness which correspond to 2 elements. The mesh with 20 mm thickness can be seen in 4.1. The brick elements of the bending critical case have a width of 31.4123 mm a height of 30.2131 mm except for the top layer of the concrete shell where the height is 35 mm. The mesh width of the shear critical model is the same as the bending critical case but the height is 25 mm due to the

height difference between the two cases. The reason for using strange dimensions and a different height at the top layer is the arrangement of the beam and solid elements in the model. The beam elements used for the reinforcements and the solid elements used for the concrete shell share the same nodes. To be able to create such a model, the nodal coordinates of elements should be arranged according to the reinforcement layout. No coupling method such as Constrained_Lagrange_in_Solid was used to model the bond between the reinforcement and the concrete. A node-sharing model was built which merges the nodes of beam elements and solid elements and assumes the perfect bond between the rebars and concrete.

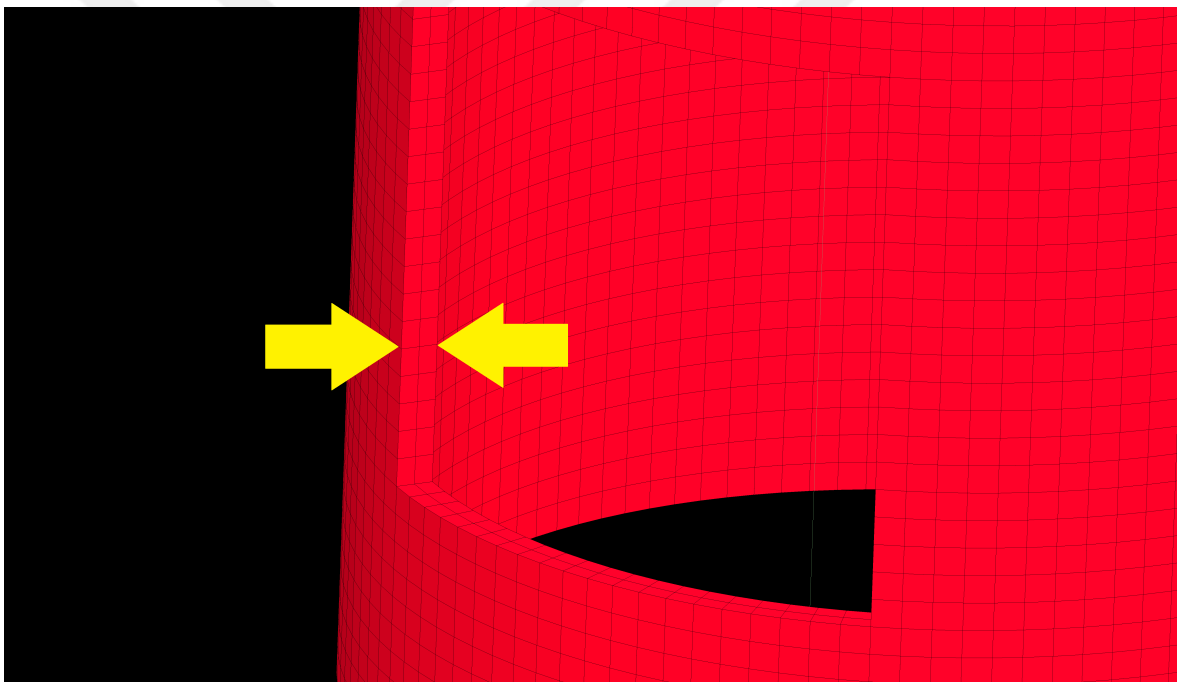

Figure 4.1. The model with 2 elements through the thickness.

The mesh dimensions of the steel tube and the cap at the top of the section are variable but the mesh resolution in these regions is not important because they were modeled as rigid elements which have zero deformation and are not considered in time step calculation. The 3D models of the bending and shear critical cases are demonstrated in Figure 4.2 and Figure 4.3, respectively.

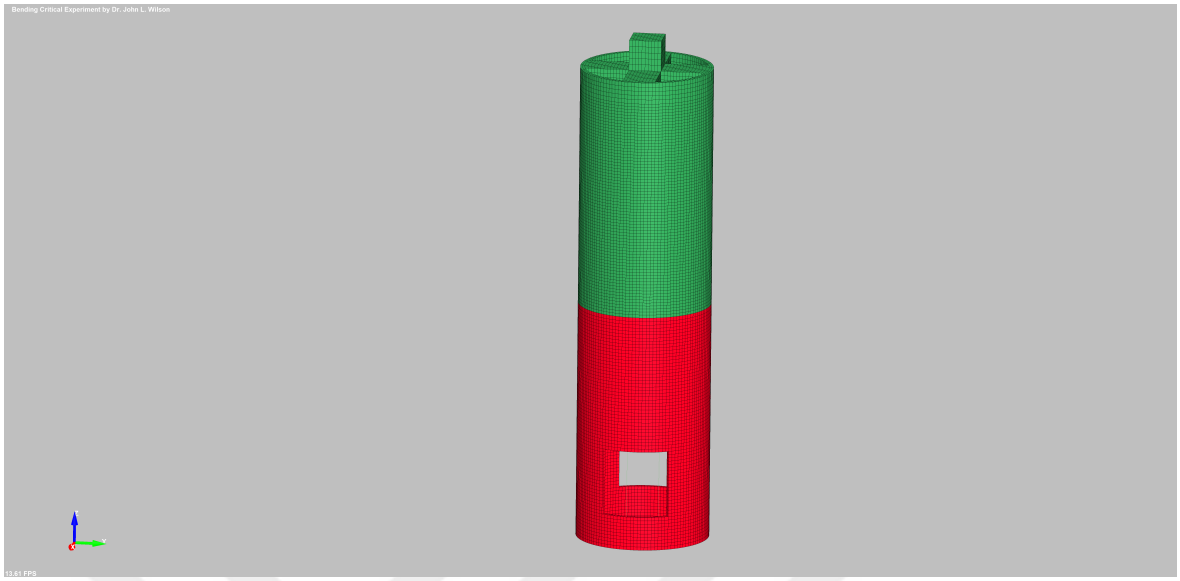

Figure 4.2. The bending critical case model.

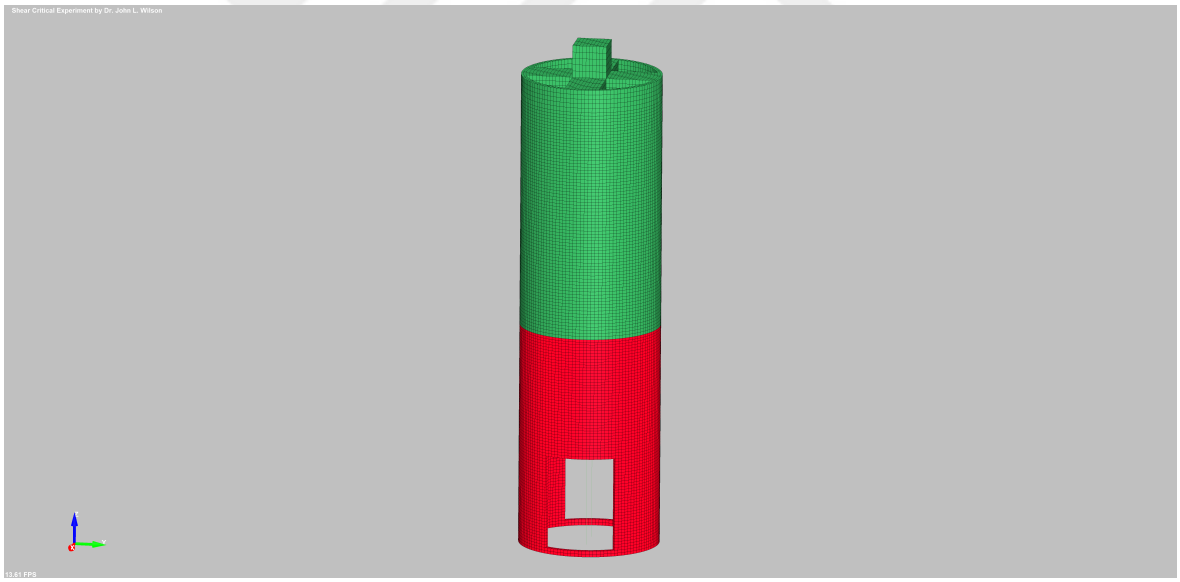

Figure 4.3. The shear critical case model.

4.2. Modeling of Rebars

There are various approaches in LS-DYNA to model the reinforcement of RC structures [22]. In this study, reinforcing rebars were modeled explicitly including the model that uses the Winfrith concrete model which has a smeared reinforcement property. Explicitly-modeled rebars can be coupled by constraint methods such Con-

strained_Lagrange_in_Solid, Constrained_Beam_in_Solid, or ALE_Coupling_Nodal Constrained, to model the interaction between reinforcing rebars and concrete. Alternatively, the meshes of solid elements for concrete and beam or truss elements for reinforcement can be modeled such that the nodes of these elements coincide. The last approach is referred to as node-sharing. Creating a node-sharing mesh of a geometrically simple structure with only longitudinal reinforcement is not a problem whereas a structure with stirrups and additional reinforcement can be quite challenging. The node-sharing approach was utilized in this study.

Due to the inability of truss elements to provide bending resistance [22], beam elements were used to model reinforcing rebars. For the element formulation, Belytschko-Schwer tubular beam with cross-section integration was chosen. 2x2 Gauss quadrature option of the element formulation was used. The reinforcement cages of the bending and shear critical case are shown in Figure 4.4 and Figure 4.5, respectively.

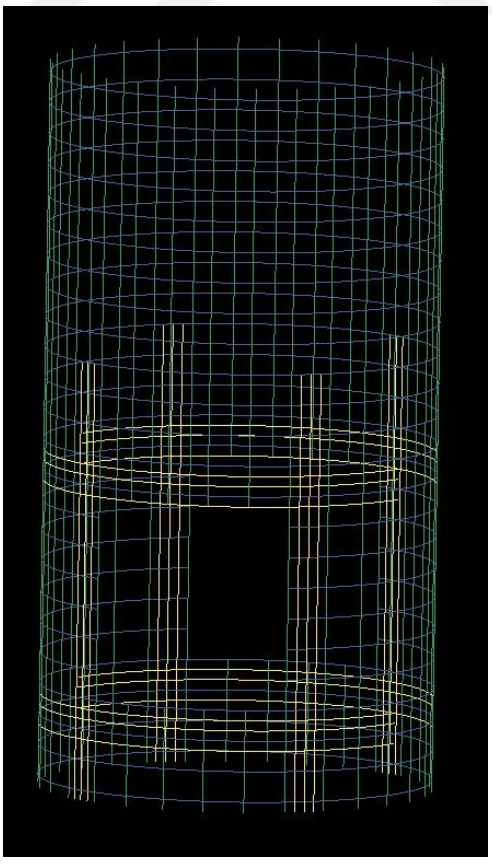

Figure 4.4. The reinforcement layout of the bending critical case.

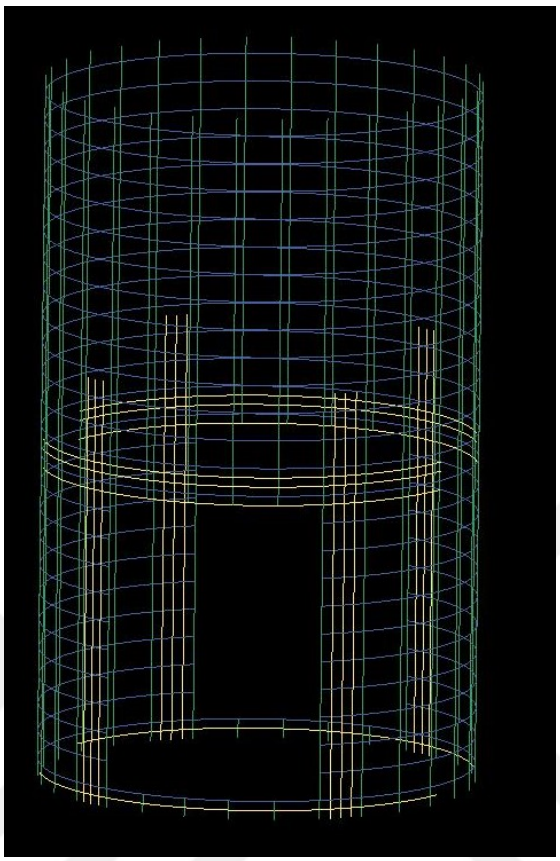

Figure 4.5. The reinforcement layout of the shear critical case.

4.3. Prestressing Tendons

To simulate the prestressing tendons, two beam elements lying top to bottom were created. The default truss element formulation was used for the prestressing tendons. The top nodes of these beam elements merged with two nodes of the steel cap to create bonding. The bottom nodes of the beams were constrained in all translational degrees of freedom. To create an axial load in the beam, ADD_THERMAL_EXPANSION keycard was used to apply thermal loading to the beams. This thermal loading was applied gradually in 0.1 seconds to limit inertial forces. The thermal loading was arranged such that the contraction of the beams creates a 116 kN axial load in each beam. Due to the merged nodes of the steel cap and the beam, the axial load in the beams was transferred to the steel cap which is a rigid part that transfers the load to the concrete shell. Having created the prestressing tendons and applied thermal

loading, the axial stresses in concrete shell elements were checked. 1.55 MPa axial stress which is the axial stress in John Wilson's experiment was created successfully.

4.4. Load Definition

In the experimental studies, displacement-controlled loadings were applied by a hydraulic actuator [11, 12]. To imitate this loading condition, prescribed motions were applied to the top-center node of the steel cap of the bending and shear critical models with the BOUNDARY_PRESCRIBED_MOTION keycard. This keycard can define nodal motions in displacement, velocity, and acceleration on a node. In this study, a displacement history was defined for each case. In Figure 4.6 and Figure 4.7, the displacement-time curves for the bending and shear critical case can be seen. Instead of changing the direction of the loading abruptly which may cause numerical problems in explicit time integration schemes, smoother curves were defined.

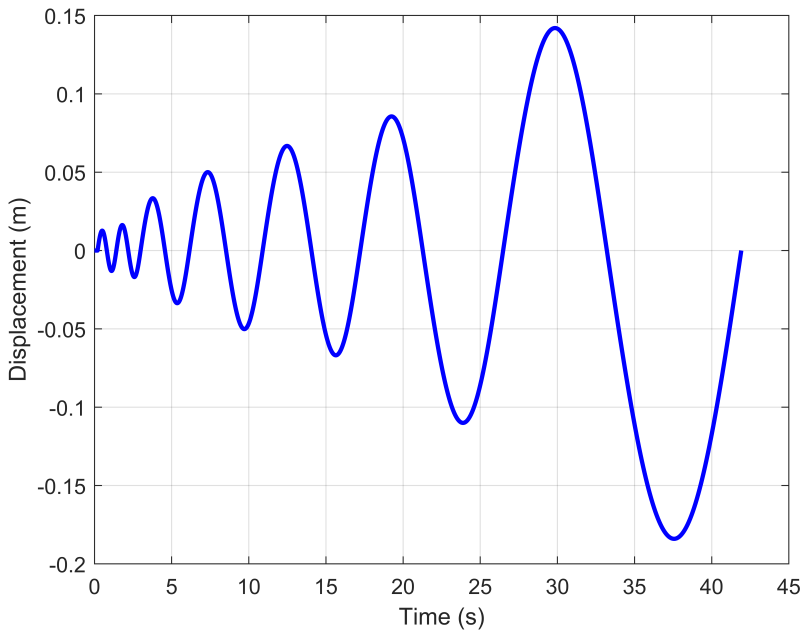

Figure 4.6. The displacement curve of the bending critical case.

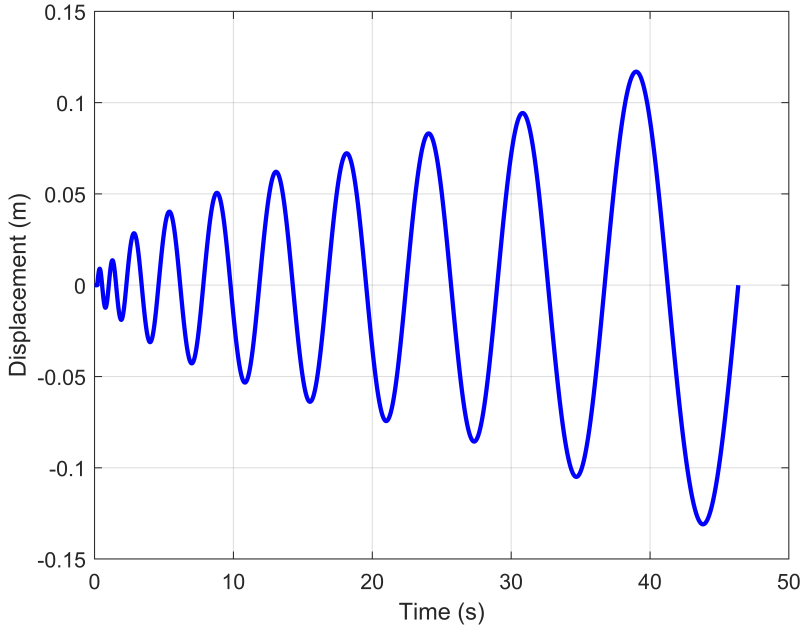

Figure 4.7. The displacement curve of the shear critical case.

4.5. Boundary Conditions

In both of the experimental setups, the pipe was supported on a reinforced concrete block which was anchored to the steel anchorage block. In the numerical models, the reinforced concrete and steel blocks were not modeled. It was assumed that the support of the pipe is rigid and the pipe was fixed perfectly. The bottom nodes of the brick elements located at the base of the pipe were constrained by the BOUNDARY_SPC_NODE keycard. All degrees of freedom of the nodes were constrained.

4.6. Material Parameters

Material models are defined with MAT keycards in LS-DYNA. Each material model keycard has many input parameters that define different properties of the material model such as compressive strength or fracture energy. The first input of all material model keycards is the material identification (MID) that is a unique number for each material defined in the model. MID input will not be mentioned in the fol-

lowing subsections. Some of the material models can work with the minimum required input parameters and the undefined parameters are generated automatically. The material models used in this study require different input parameters to work. In the following subsection, the input parameters will be discussed and the used values will be specified.

LS-DYNA is not a unit-aware software which means the user should use a consistent set of units for all inputs. The units in this study were listed in Table 4.2.

Table 4.2. The consistent units used.

Mass	kg
Length	m
Time	s
Force	N
Stress	Pa
Energy	J

4.6.1. MAT_072R3 K&C

The Karagozian & Case (K&C) concrete model has 49 input parameters. The model has the capability of generating model parameters from the unconfined compressive strength of the concrete. To use this feature of the model, the A0 input parameter should be set to the unconfined compressive strength of the concrete and it should be negative. The used input parameters for the K&C model are listed in Table 4.3. RO is the density of the concrete, PR is the Poisson ratio, and LOCWID is three times the maximum aggregate diameter. RSIZE and UCF are conversion factors that convert the user units to the units of the material model. Due to the troublesome work required to calibrate the K&C model, the model was used with the minimum number of input parameters.

Table 4.3. The input parameters of K&C model.

Parameter	**Value**
RO	2500
PR	0.17
A0	-4.00E+07
RSIZE	39.371
UCF	1.45E-04
LOCWID	0.03

4.6.2. MAT_084 Winfrith

The Winfrith material model has 30 input parameters four of which define the rebar properties. If the rebars are modeled explicitly, these four parameters are not required.

RATE parameter determines the rate effects and has three options. If the Rate parameter is equal to 0, the rate effects are included and the FE parameter should be set to the fracture energy of the concrete. In the case of the other two options, when the RATE is equal to 1 or 2, the strain rate effects are turned off and the FE parameter should be equal to the crack width (w) at which crack-normal tensile stress goes to zero. The difference between the RATE=1 and RATE=2 is in terms of the crack algorithm. RATE 2 option uses an improved crack algorithm. The fracture energy of the concrete was not available in the experimental study. To calculate the fracture energy, the formula of the CEB-FIP Model Code 90 [23] defined in Equation (4.1) was used. The maximum aggregate size of the concrete is 10 mm. G_{Fo} value for 10 mm aggregate size was linearly interpolated.

$$G_F = G_{Fo}\left(\frac{f_{cm}}{f_{cmo}}\right)^{0.7} \tag{4.1}$$

where G_F is the fracture energy in N/mm, G_{Fo} is the base value of fracture energy which depends on maximum aggregate size, f_{cm} is the mean concrete compressive strength in MPa, and f_{cmo} is a constant and is equal to 10 MPa.

The relationship between the fracture energy and the crack width at which crack-normal tensile stress goes to zero was defined in [24] and the strain softening response of concrete is assumed to be linear. Therefore the area under the tensile stress versus the crack width curve can calculate easily. The relation of the crack width with the fracture energy and tensile strength is defined as

$$w = \frac{2G_F}{f'_t} \cdot \tag{4.2}$$

The uniaxial tensile strength of the concrete was calculated according to the recommendation made in [11]. For the initial tangent modulus of the concrete, FIB Model Code 90 was used. The summary of the input parameters of the Winfrith model can be seen in Table 4.4.

Table 4.4. The input parameters of Winfrith model.

Parameter	**Values**
RO	2500
TM	3.50E+10
PR	0.17
UCS	4.00E+07
UTS	3.20E+06
FE for RATE=1 or 2	4.25E-05
FE for RATE=0	6.80E+01
ASIZE	5.00E+00

To be able to evaluate the parameters' sensitivity, alternative values of each parameter were determined. The alternative values are listed in Table 4.5.

Table 4.5. The alternative input parameters of Winfrith model.

Parameter	**Values**
TM	1.80E+10
UCS	2.50E+01
UTS	2.00E+00
FE for RATE=0	5.00E+01
ASIZE	1.00E+01

4.6.3. MAT_159 CSCM

The first option of the CSCM model work with a total of 45 input parameters. On the other hand, the second option, which uses default parameters for normal strength concrete, requires 11 input parameters. Only 3 of these input parameters are related to the properties of the concrete which are the unconfined compressive strength, the maximum aggregate size, and mass density. The rate effects option was turned off. The CSCM model has an in-built erosion option which is based on the damage and the maximum principal strain limit defined by the user. The erosion option of the model was not used. The used parameters are summarized in Table 4.6.

Table 4.6. The input parameters of CSCM model.

Parameter	**Value**
RO	2500
FPC	4.00E+07
DAGG	0.01

4.6.4. MAT_272 RHT

The RHT material model has 38 input parameters. For the simulations with the RHT concrete model, the parameters defined are the mass density and the compressive strength. The model can generate the remaining parameters from the compressive strength of the concrete by interpolating the values between 35 MPa and 140 MPa. If the FC parameter is set to 0, the compressive strength is assumed to be 35 MPa. The list of used parameters for the RHT model is shown in Table 4.7.

Table 4.7. The input parameters of RHT model.

Parameter	**Value**
RO	2500
FC	4.00E+07

4.6.5. MAT_24 for Rebar

The Piecewise Linear Plasticity model has a total of 4 keycards and 28 input parameters 16 of which are used for defining the effective plastic strains and the corresponding yield stresses. The effects of the SIGY, and ETAN parameters were assessed by using two different parameters for each. In the experimental study, the yield strength, the 3% strain strength, and the failure strength of the rebars were given. The stress-strain curve of the rebars was defined by a bilinear curve using the ETAN input parameter which defines the tangent modulus. For the ETAN input parameter, 0.9 GPa and 0.4 GPa were used. All used values for the SIGY, and ETAN and the remaining parameters are listed in Table 4.8.

Table 4.8. All input parameters of MAT_24 model.

Parameter	**Value**
ETAN	0.9 or 0.4 GPa
SIGY	530 or 430 MPa
RO	7800
PR	0.3

5. SIMULATION RESULTS

In the following sections, the simulation results with different material models were compared with the experimental results for the bending critical case and the shear critical case, respectively. The effect of the input parameters of the Winfrith concrete model was discussed in detail. Lastly, the optimum simulation parameters for each model was presented.

5.1. Bending Critical Case

5.1.1. MAT_072R3 K&C Results

The force-displacement curves of the experimental study and the model with MAT_072R3 were compared in Figure 5.1. The numerical model initially behaved in a more stiff manner and overpredicted the first peak strength by more than 20% but when the loading changed the direction, the model caught the second peak accurately. The numerical model started to lose strength immediately after the first cycle with a decreasing trend until the third cycle whereas the experimental result showed an increasing trend in the strength up to the fourth cycle. Later, the model began to gain strength after the third cycle and continued in this manner to the end of the simulation. The envelopes of the force-displacement curves can be seen in Figure 5.2.

It is obvious that the K&C model did not predict the overall response of the chimney section. Within the linear elastic region, the model can produce reasonable results but when nonlinearity comes into play, the model underestimates the peak strength values. The K&C model also cannot catch the pinching behavior and has a different hysteresis shape. The stiffness degradation is more severe in the numerical model. Additionally, the model did not fail under this loading.

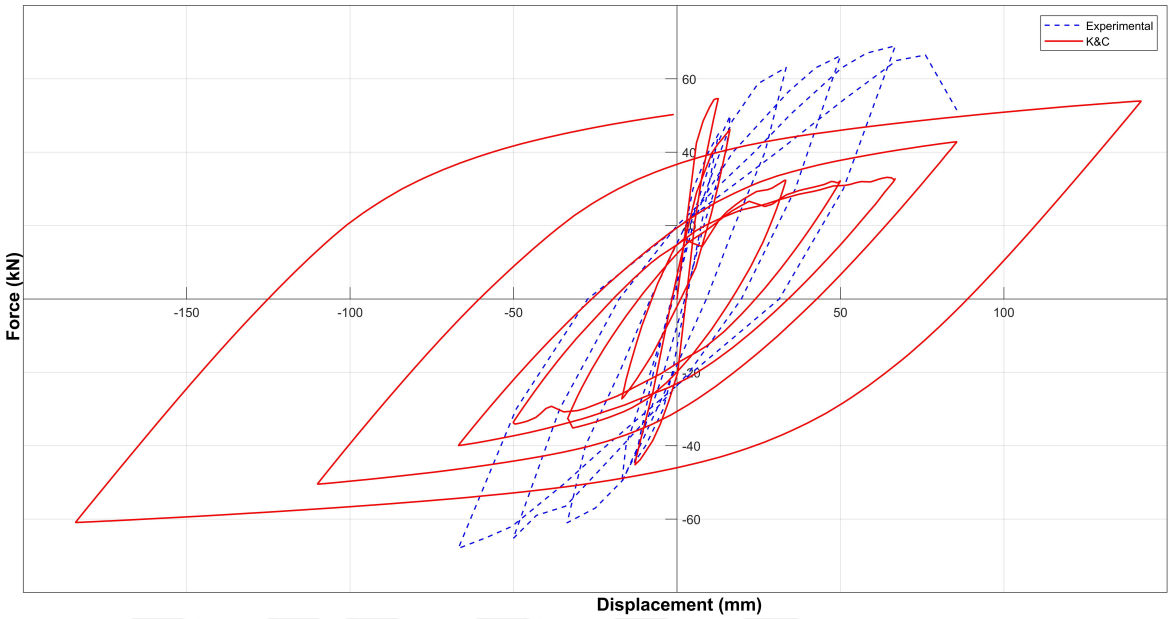

Figure 5.1. The comparison of the K&C model with bending critical test result.

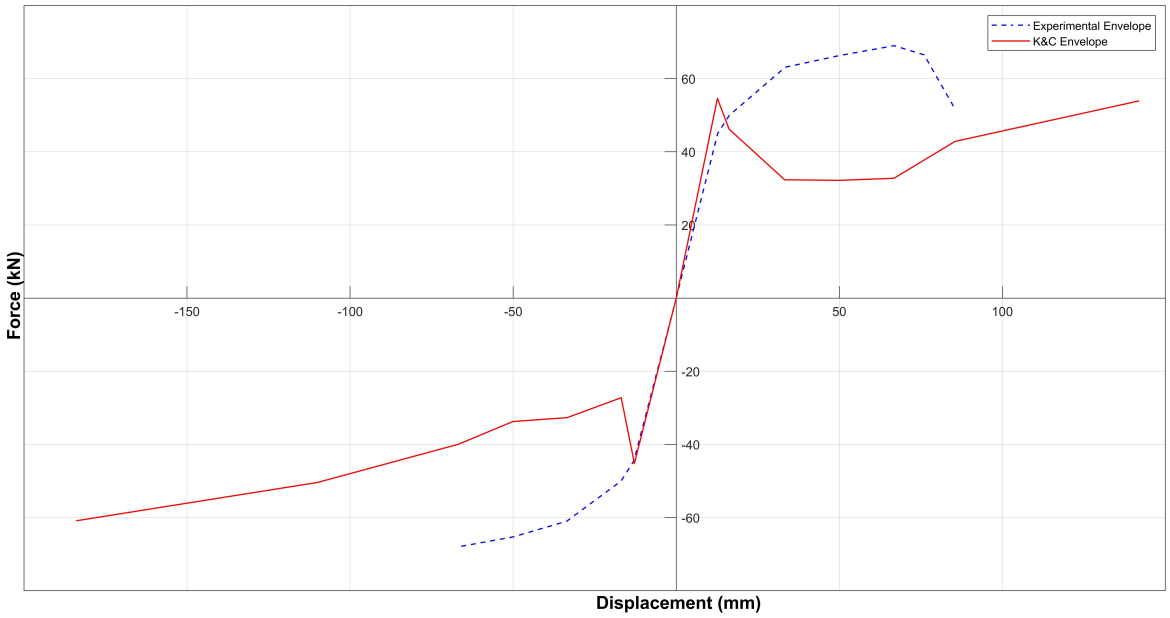

Figure 5.2. The envelope curves of the K&C model and bending critical test result.

5.1.2. MAT_084 Winfrith Results

For the Winfrith model, firstly the rate effects were turned off and the RATE parameter was set to 1. In Figure 5.3, the hysteresis curves of the Winfrith model with the RATE=1 and the bending critical test result were compared. The model overpredicted the first peak load by 38%. The difference between the predicted and measured peak loads for the remaining cycles decreased compared to the first cycle and was in the range of 20%. Figure 5.4 shows the envelopes of the hysteresis curves. The model showed pinching behavior similar to the experimental result. The slopes of the loading and unloading curves are steeper compared to the experimental results but have a similar trend. The model can complete the six cycles whereas the bending critical chimney failed around the peak load of the sixth cycle.

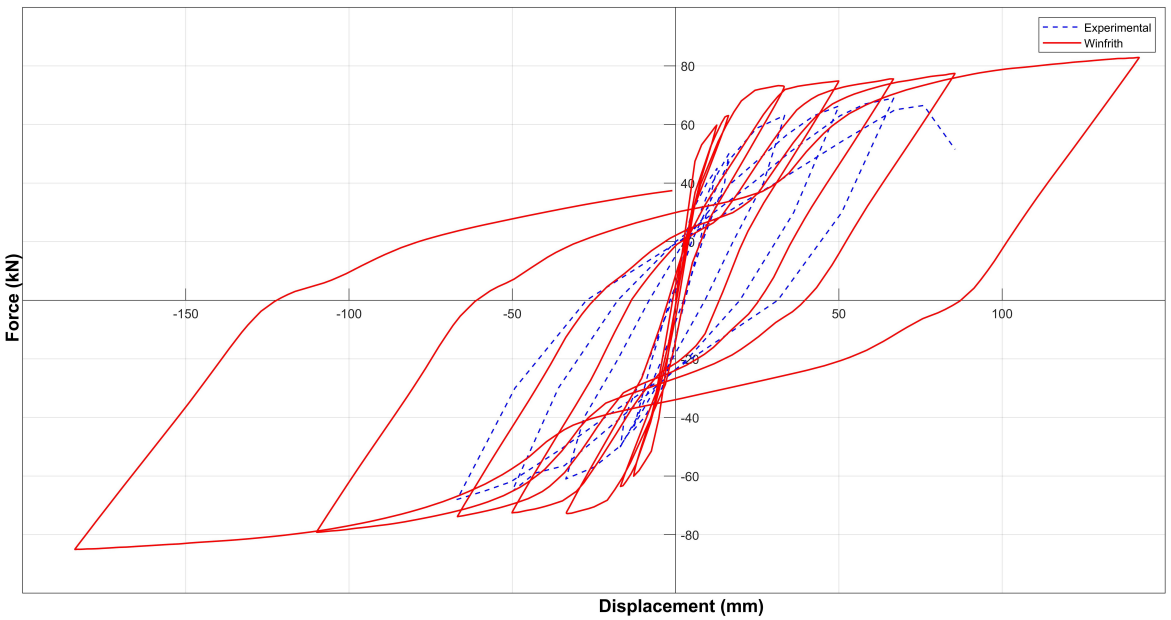

Figure 5.3. The comparison of the Winfrith RATE=1 model with bending critical test result.

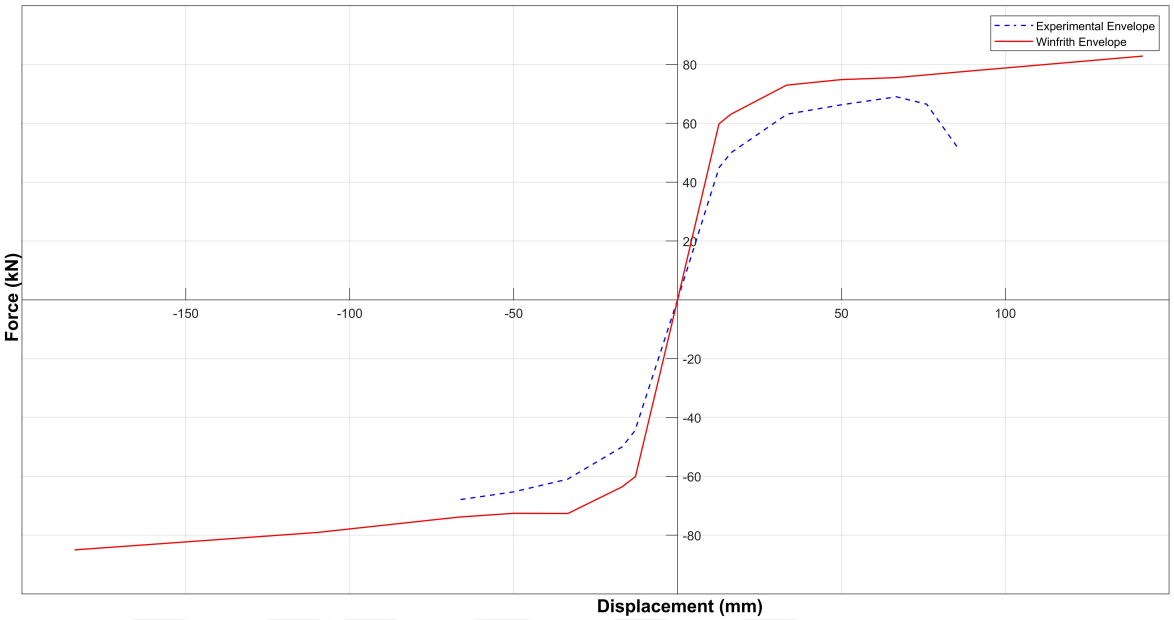

Figure 5.4. The envelope curves of the Winfrith RATE=1 model and bending critical test result.

The comparison of the model with the RATE=1 and the model with the RATE=2 is shown in Figure 5.5. Both models ignore strain rate effects and all remaining input parameters are the same. The peak loads of the RATE=2 model are higher more than 10% on average. The RATE=2 model is stiffer compared to the RATE=1 model and showed less pinching. Figure 5.6 shows the envelope curves for the Winfrith with RATE=2 and the bending critical test result.

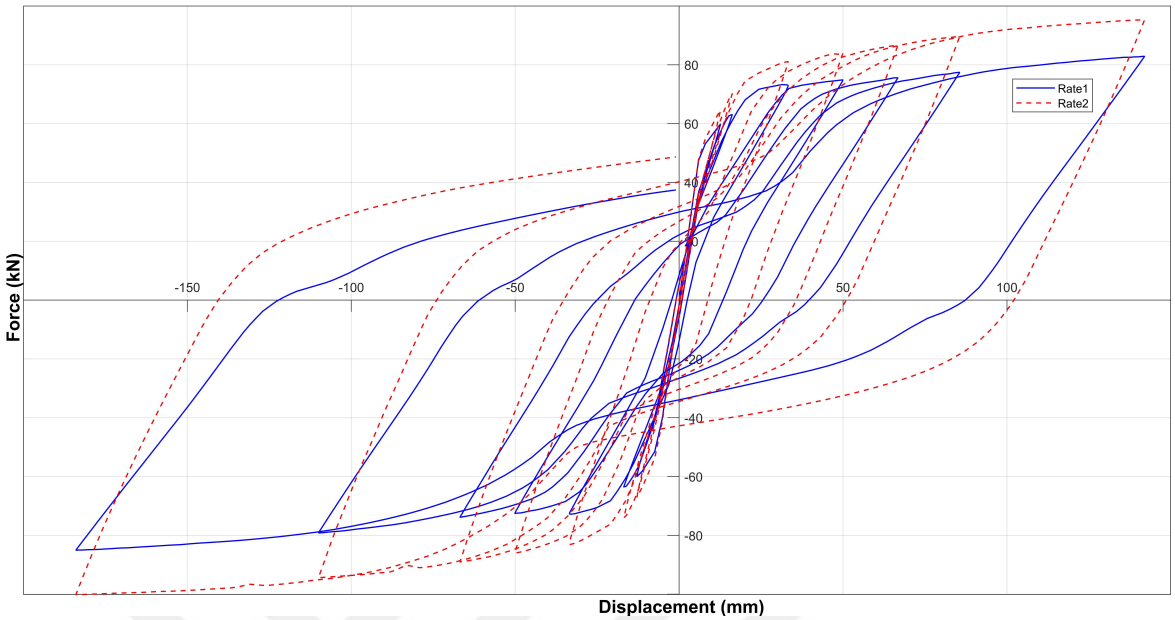

Figure 5.5. The comparison of the Winfrith models with RATE=1 and RATE=2.

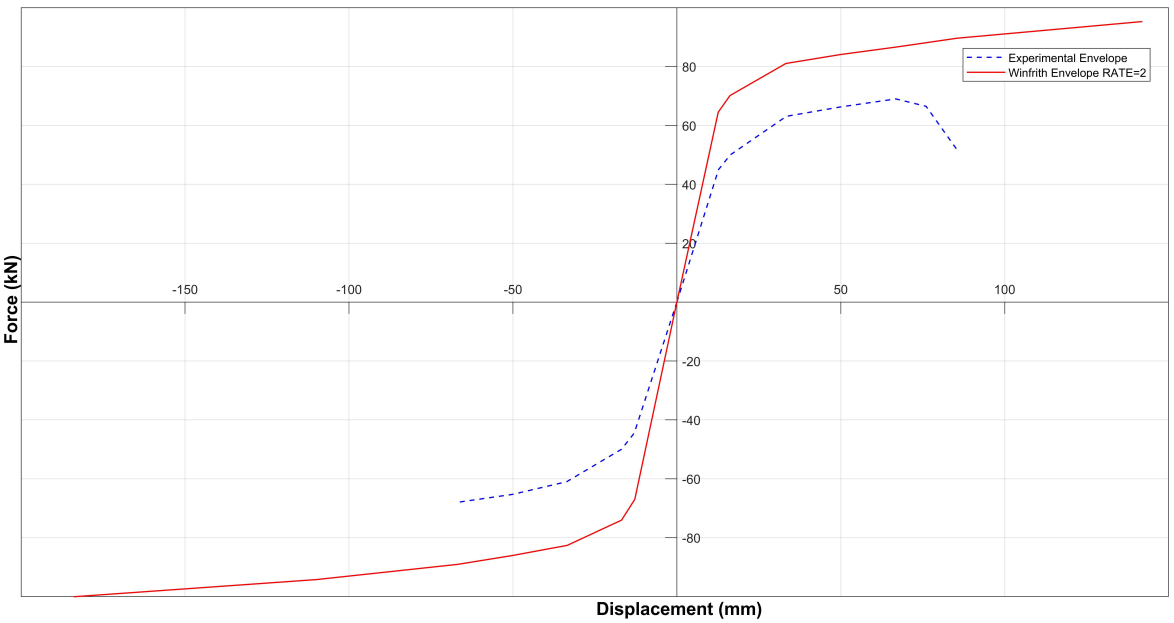

Figure 5.6. The envelope curves of the Winfrith RATE=2 model and bending critical test result.

The first peak load of the model that includes strain rate effects (RATE=0) is smaller compared to the model with the RATE=1 by 57%. After the second cycle, the model with the RATE=0 and RATE=1 gave similar results. Figure 5.7 shows the comparison of the two models. The RATE=0 model showed steeper unloading slopes

relative to the RATE=1 model. The pinching is more severe when the RATE=1. The comparison of the envelope curves of the Winfrith model with RATE=0 and the bending critical case is shown in Figure 5.8.

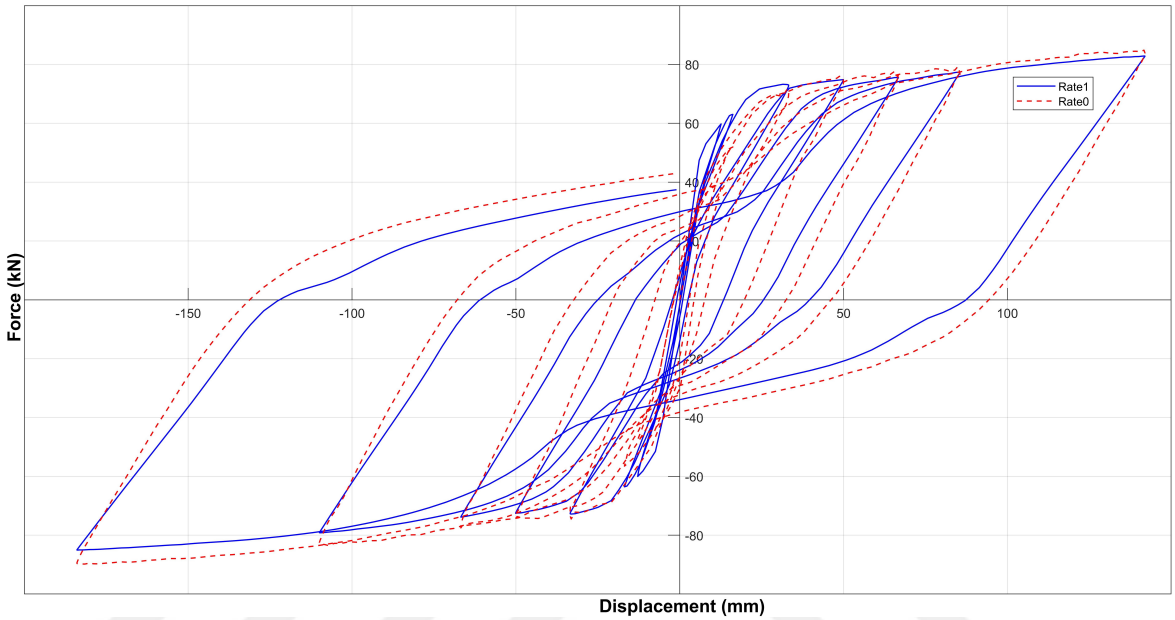

Figure 5.7. The comparison of the Winfrith models with with RATE=1 and RATE=0.

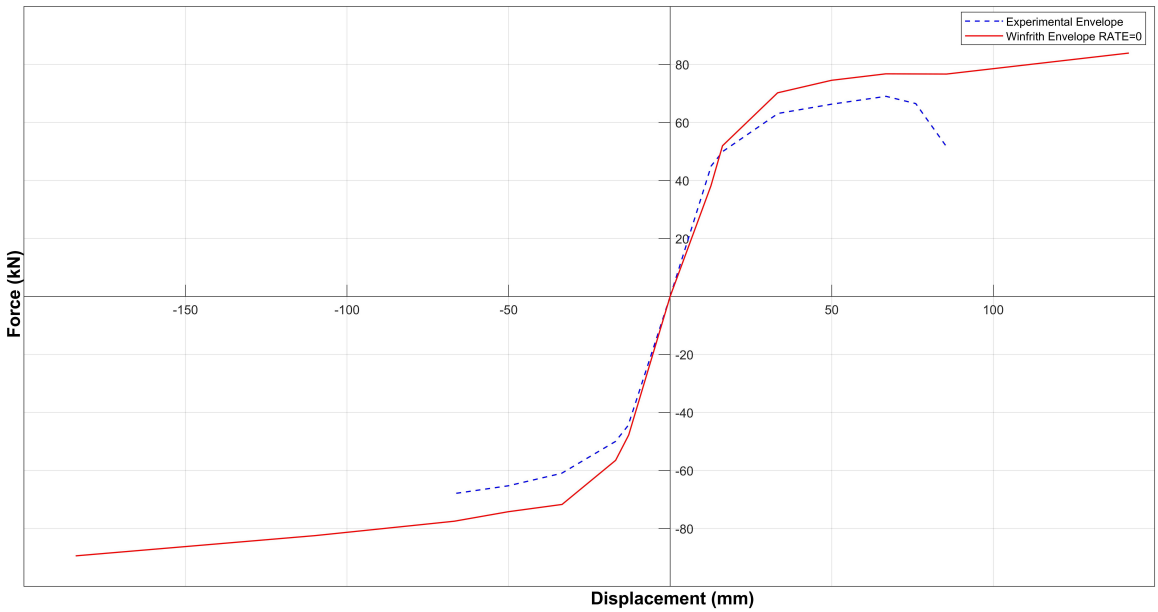

Figure 5.8. The envelope curves of the Winfrith RATE=0 model and bending critical test result.

When the RATE=0, the FE parameter defines the fracture energy of the concrete. Two different values, 50 N/m and 68 N/m, were used to evaluate the effect of fracture energy. The comparison of the two models is shown in Figure 5.9. The effect of the fracture energy in terms of peak loads is less than 3% which is negligible. The loading and unloading slopes are similar and the slopes decrease with decreasing fracture energy.

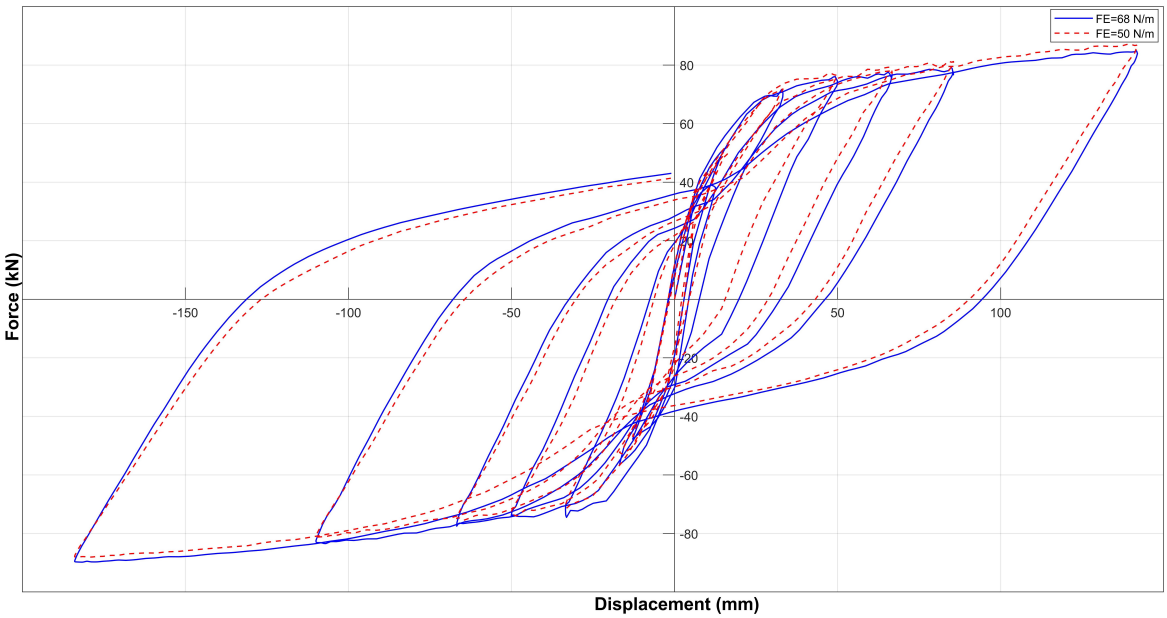

Figure 5.9. The comparison of the Winfrith models with different fracture energy.

Figure 5.10 compares the Winfrith concrete models with two different maximum aggregate size input parameters, 5 mm and 10 mm. Although the maximum aggregate size doubled, the curves are nearly identical and the effect of the ASIZE parameter is negligible. When the maximum aggregate size of the concrete is unknown, using an average value does not affect the model's accuracy in a major way.

The effect of the tensile strength (UTS) of the concrete can be seen in Figure 5.11. The model with a tensile strength of 3.2 MPa responded slightly stiffer in the first three cycles compared to the low tensile strength model but the difference between peak loads is not greater than 13%. For the remaining cycles, the peak loads are very close to each other. The pinching behavior is more serious for the model with 2 MPa tensile

strength. These are expected results because the stiffness degradation and pinching are related to the cracking of concrete which is affected by the tensile capacity.

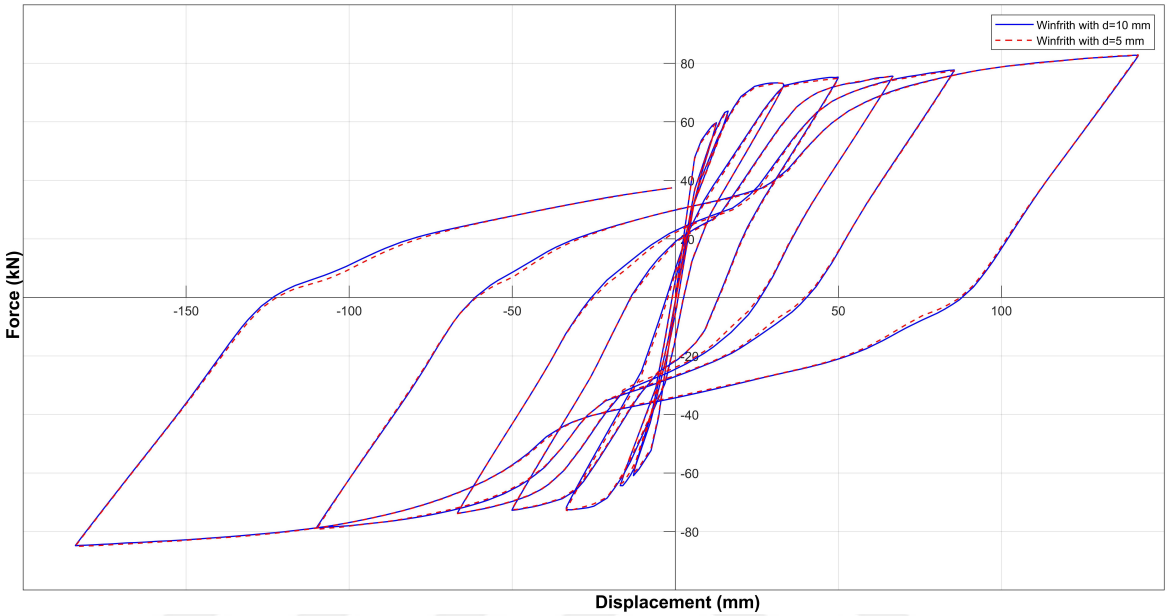

Figure 5.10. The comparison of the Winfrith models with different maximum aggregate sizes.

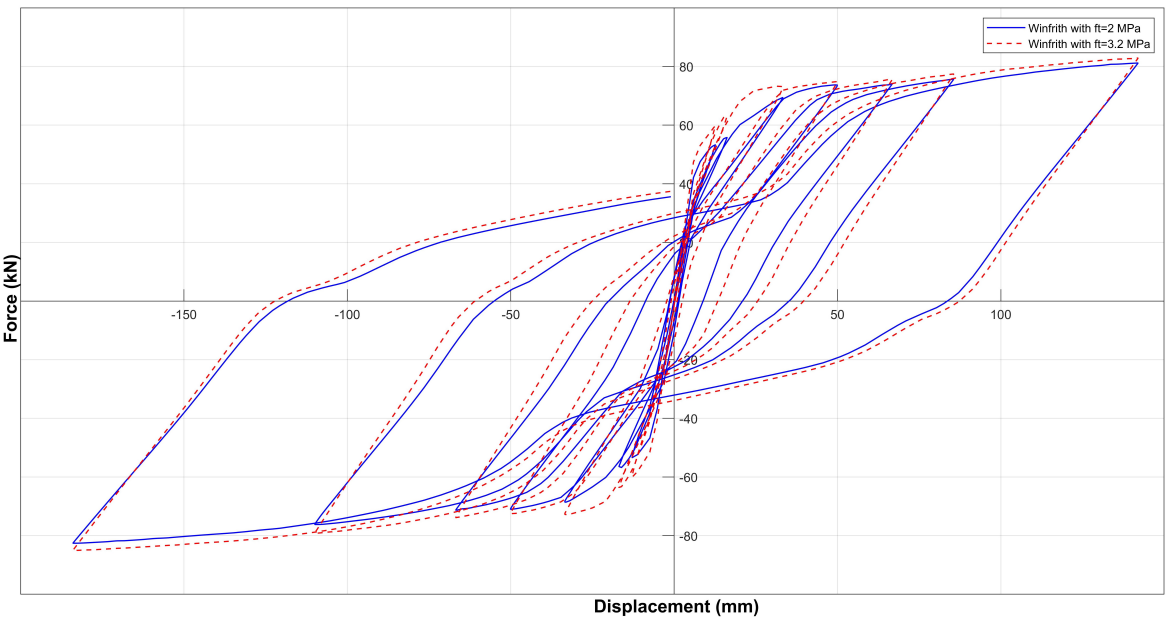

Figure 5.11. The comparison of the Winfrith models with different concrete tensile strengths.

The decrease in the elastic modulus (TM) of the concrete has a similar effect to tensile strength degradation on the peak loads. The differences between peak loads of the two models with different elastic modulus are within 10%. The comparison of the models with 35 GPa and 18 GPa elastic modulus was demonstrated in Figure 5.12. The pinching of the model with 18 GPa elastic modulus is more serious relative to the model with 35 GPa elastic modulus but it was not as severe as the low tensile strength model. The effect of the elastic modulus degradation is decreasing with increasing plasticity.

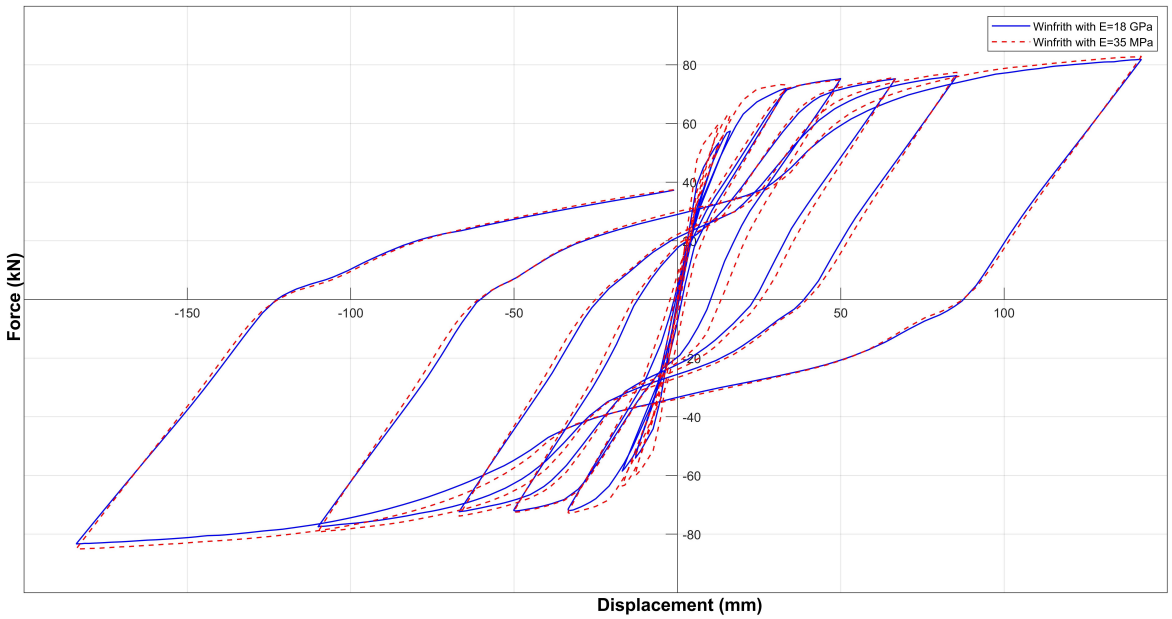

Figure 5.12. The comparison of the Winfrith models with different elastic moduli.

To be able to evaluate the effect of uniaxial compressive strength of the concrete (UCS), two models with the same input parameters except UCS were created. One of the models has a compressive strength of 40 MPa and the other has 25 MPa. The force-displacement curves of the models were compared in Figure 5.13. The two models produced nearly identical results for the first three cycles. The difference between the peak loads was less than 3% for the remaining cycles. Lastly, the loading-unloading slopes and the pinching behavior are similar.

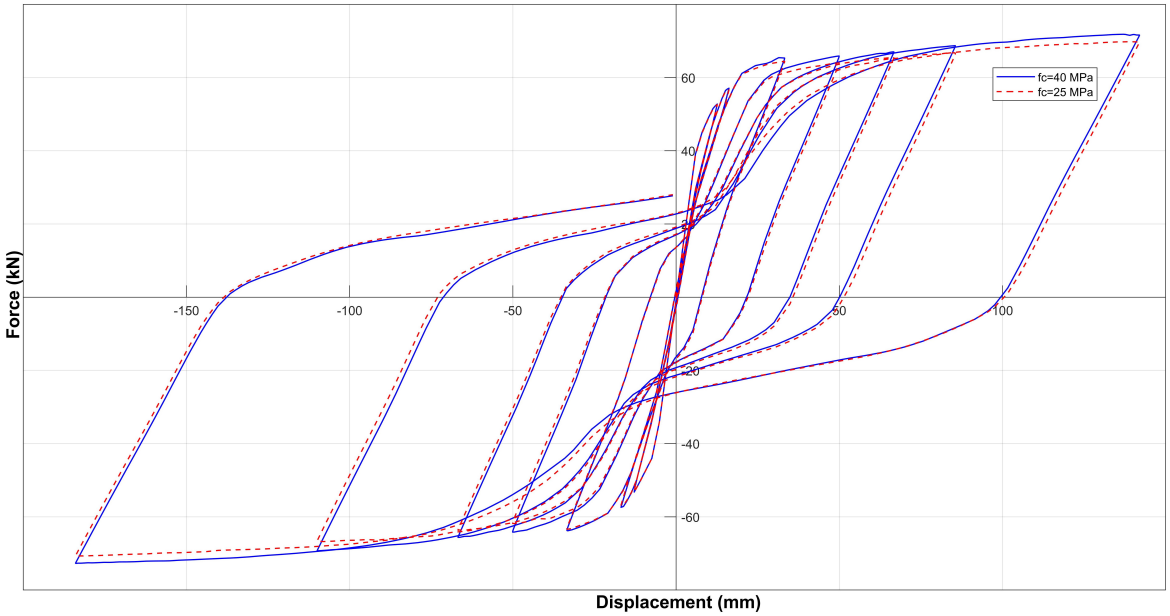

Figure 5.13. The comparison of the Winfrith models with different f_c.

The effects of input parameters of the MAT_024 were investigated. First, two different tangent moduli, 0.4 GPa and 0.9 GPa, were used. In Figure 5.14, the force-displacement curves of the two models were shown. The models showed very similar results especially for the first three cycles as expected. The tangent modulus defines the slope of the bilinear stress-strain curve after the yielding. Before the yielding of the rebars, the two models are identical. The effect of the tangent modulus might become important if the structure reaches large drift ratios. Due to the limited ductility capacity of RC chimneys, the tangent modulus did not affect the results much.

However, the yielding stress of the rebars affects the results. The comparison of the two model with different yielding stresses is shown in Figure 5.15. When the yielding stress decreased by 20%, from 530 MPa to 430 MPa, the peak loads reduced 10% on average except for the first two cycles where the response was dominated by the concrete. The unloading slopes of the two model are similar. The model with 430 MPa yielding stress showed more severe pinching.

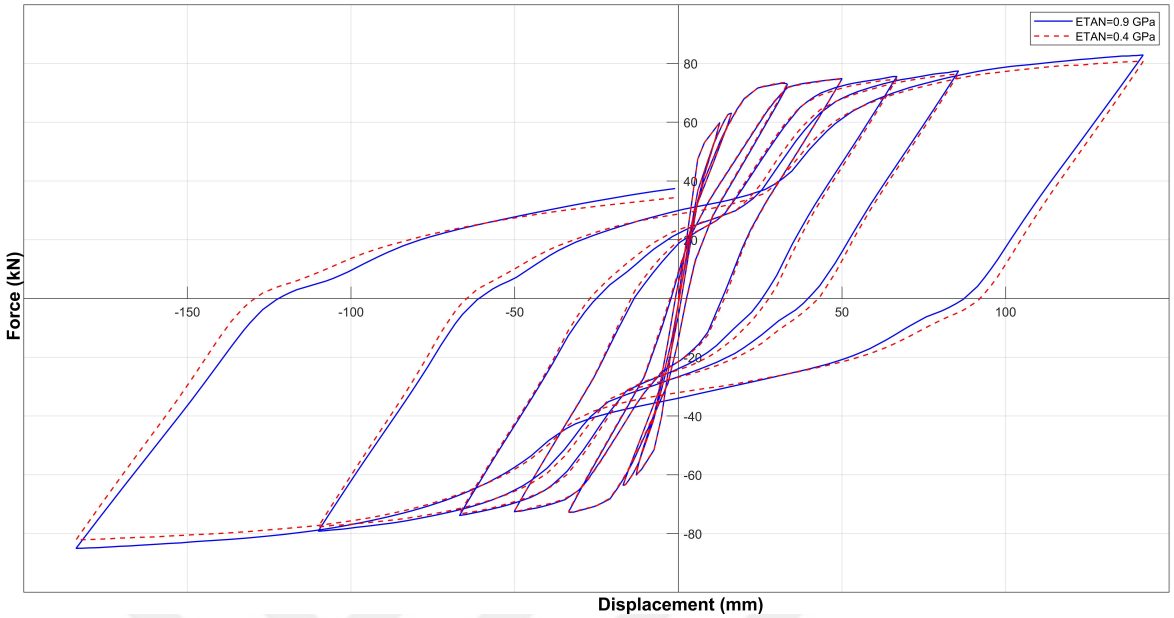

Figure 5.14. The comparison of the models with different tangent moduli.

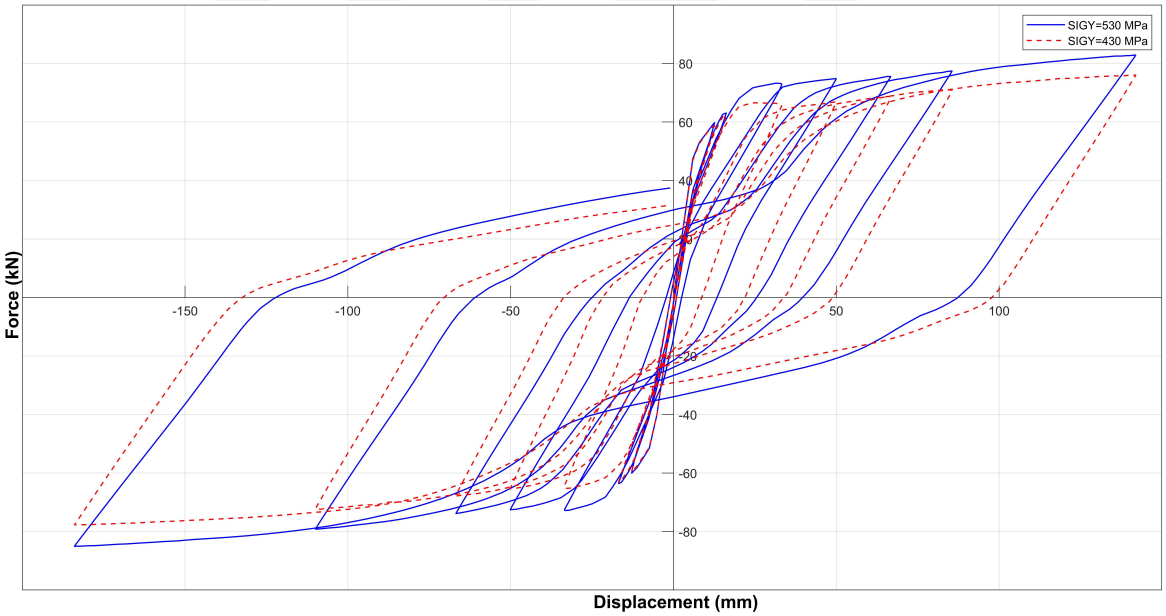

Figure 5.15. The comparison of the models with different yielding stresses.

5.1.3. MAT_159 CSCM Results

Figure 5.16 shows the comparison of CSCM results with the experimental result. The model slightly overpredicted the first peak load by about 10%. In the second cycle, the peak load was overestimated again by more than 20%. The estimated peak loads

during the third and fourth cycles are close to the measured loads. The envelopes of the force-displacement curves are depicted in Figure 5.17. The loading and unloading slopes of the model are steeper compared to the experimental result. There is no pinching at all. Steeper unloading slopes and the lack of pinching increase the area under the force-displacement curve which is equal to the dissipated energy during the loading.

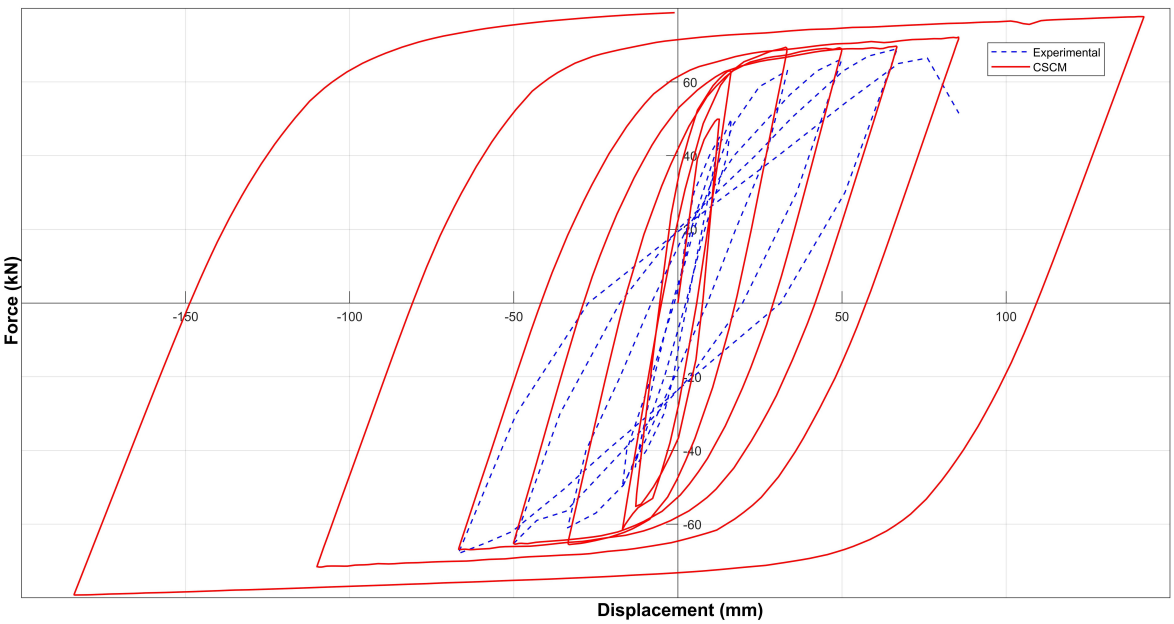

Figure 5.16. The comparison of the CSCM with bending critical test result.

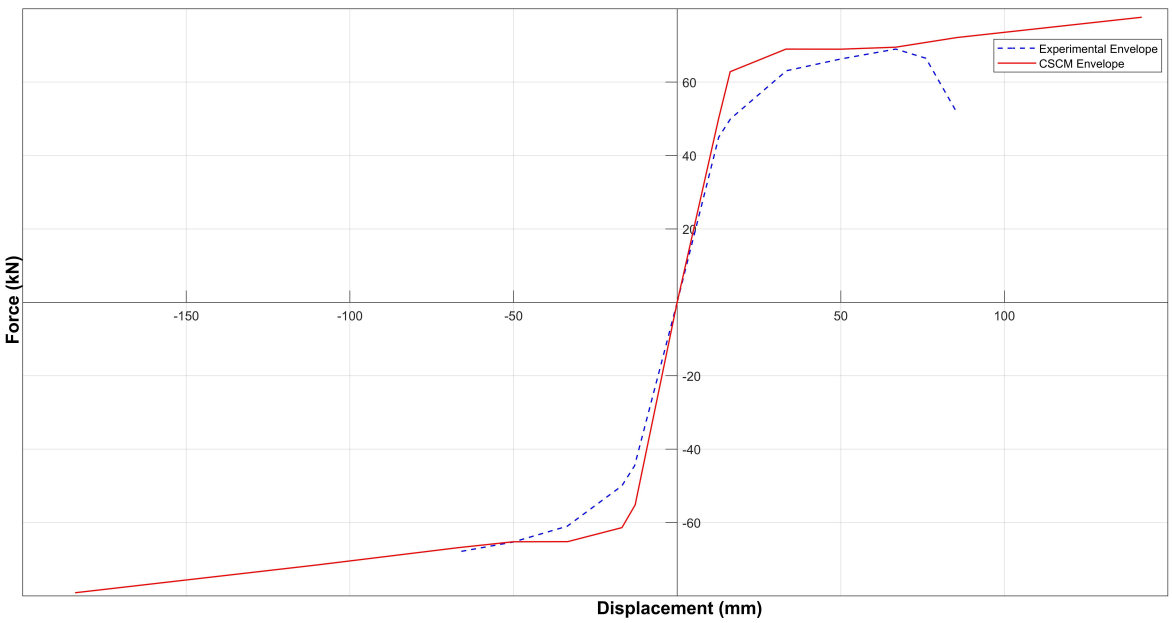

Figure 5.17. The envelope curves of the CSCM and bending critical test result.

The peak loads of the CSCM are similar to the experimental results but the shape of the hysteresis curve is different. Additionally, after the fourth cycle, the model continued to gain strength, probably due to the hardening of the reinforcement, in a linear fashion and did not fail within the simulation time.

5.1.4. MAT_272 RHT Results

The hysteresis curve of the RHT model compared with the experimental result is demonstrated in Figure 5.18. The model significantly overpredicted the first peak load by 68% The model showed a slight strength loss in the fifth cycle while the peak load of the experimental result during the fifth cycle increased relative to the previous cycle. In Figure 5.19, the envelopes of the hysteresis curves are shown.

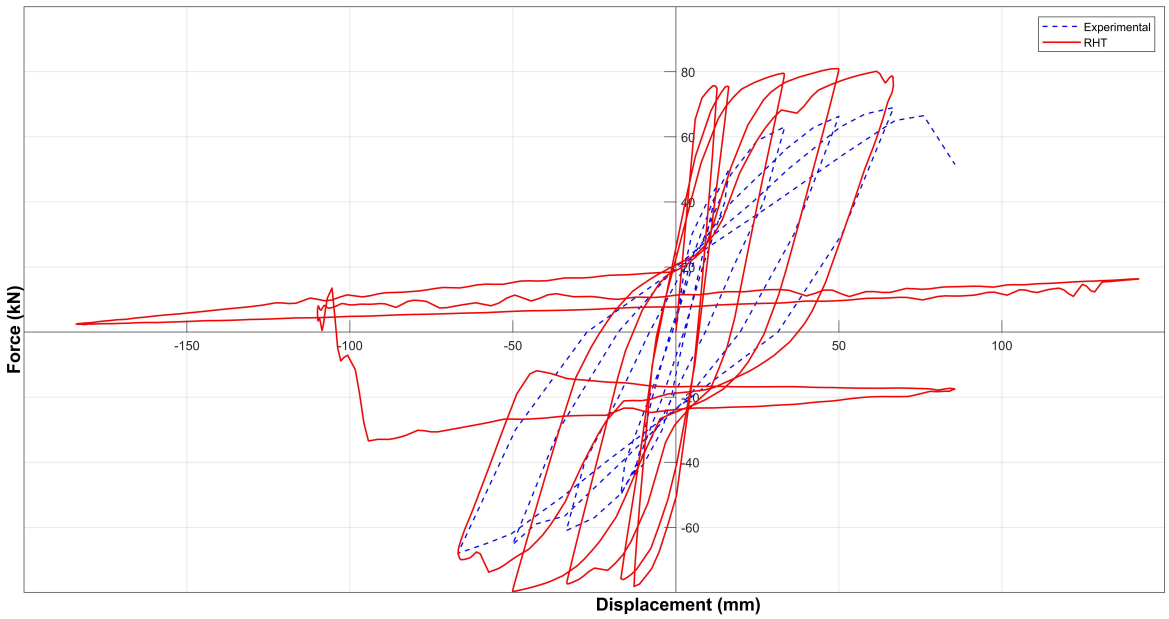

Figure 5.18. The comparison of the RHT model with bending critical test result.

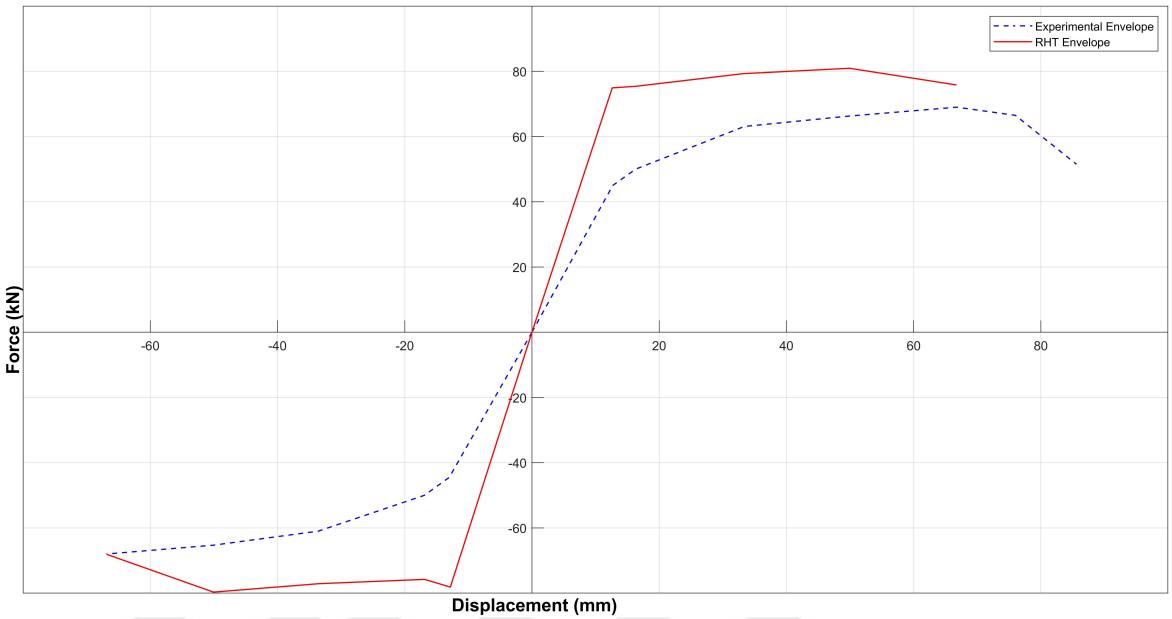

Figure 5.19. The envelope curves of the RHT model and bending critical test result.

The RHT model overestimated the peak values for every cyclic and the stiffness degradation was slower than the experimental results. However, the model showed the pinching behavior to some extend. The envelope of the numerical model was similar to the experimental result. The model failed just before the end of the fifth cycle and the failed model can be seen in Figure 5.20. The failure started at the base of the opening.

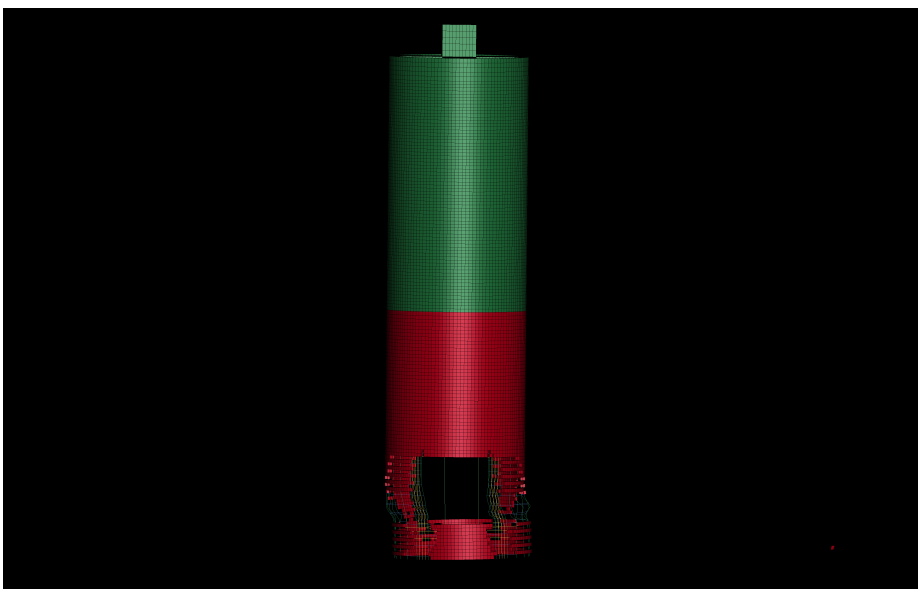

Figure 5.20. The failed RHT model for the bending critical case.

5.2. Shear Critical Case

5.2.1. MAT_072R3 K&C Results

The comparison of the shear critical case's force-displacement curves of the experimental result and the K&C model was illustrated in Figure 5.21. The initial stiffness of the numerical model is 58% higher compared to the experimental result. When the loading changed the direction in the first cycle, the model lost strength at halfway. The strength loss continued till the third cycle, whereas the experimental result showed no strength loss until the last cycle. The envelopes of the force-displacement curves can be seen in Figure 5.22.

The K&C model underestimated peaks load except the first one. A premature strength loss was observed. The predicted stiffness degradation is more serious than the experimental result. No pinching was predicted by the model and the model did not fail at the end of the simulation. Consequently, the general response of the chimney section cannot be captured.

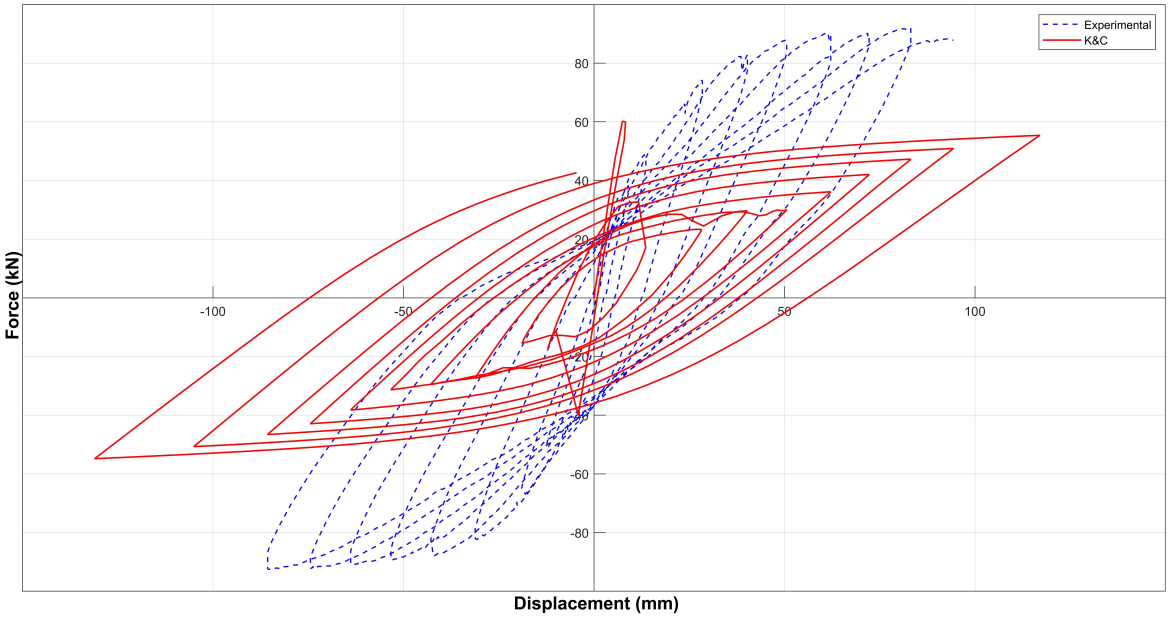

Figure 5.21. The comparison of the K&C model with shear critical test result.

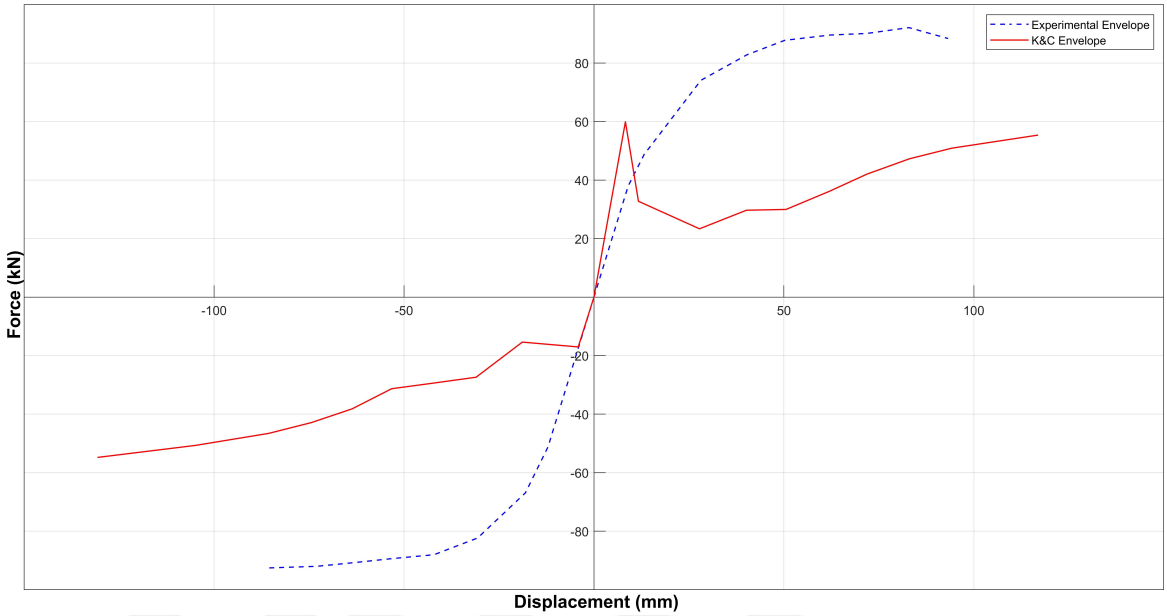

Figure 5.22. The envelope curves of the K&C model and shear critical test result.

5.2.2. MAT_084 Winfrith Results

Figure 5.23 shows the comparison of the Winfrith model with the RATE=1 and the experimental results for the shear critical case. The model overestimated the peak loads of the first four cycles. The difference between the first peak loads of the model and the experimental results decreased in every cycle and the model caught the peak load in the second peak of the fourth cycle. Figure 5.24 shows the envelopes of the hysteresis curves. The model showed pinching behavior similar to the experimental result but the pinching is more severe compared to the measured result when the displacement goes from positive to negative. The slopes of the loading and unloading curves of the model are similar to the experimental result. The model can complete the ten cycles whereas the shear critical chimney failed around the peak load of the ninth cycle.

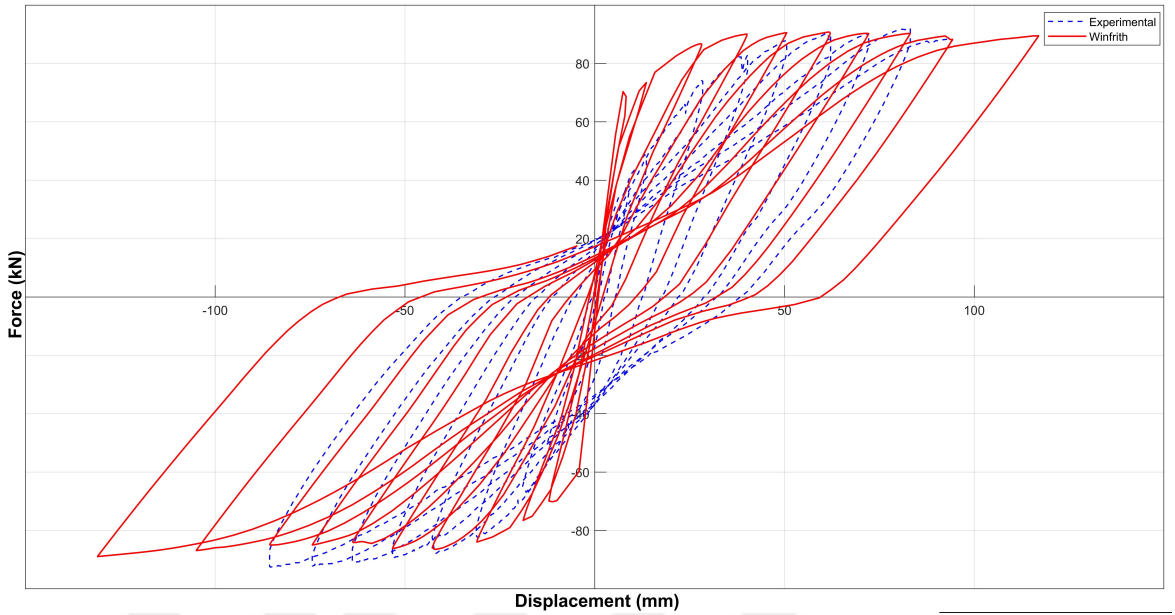

Figure 5.23. The comparison of the Winfrith RATE=1 model with shear critical test result.

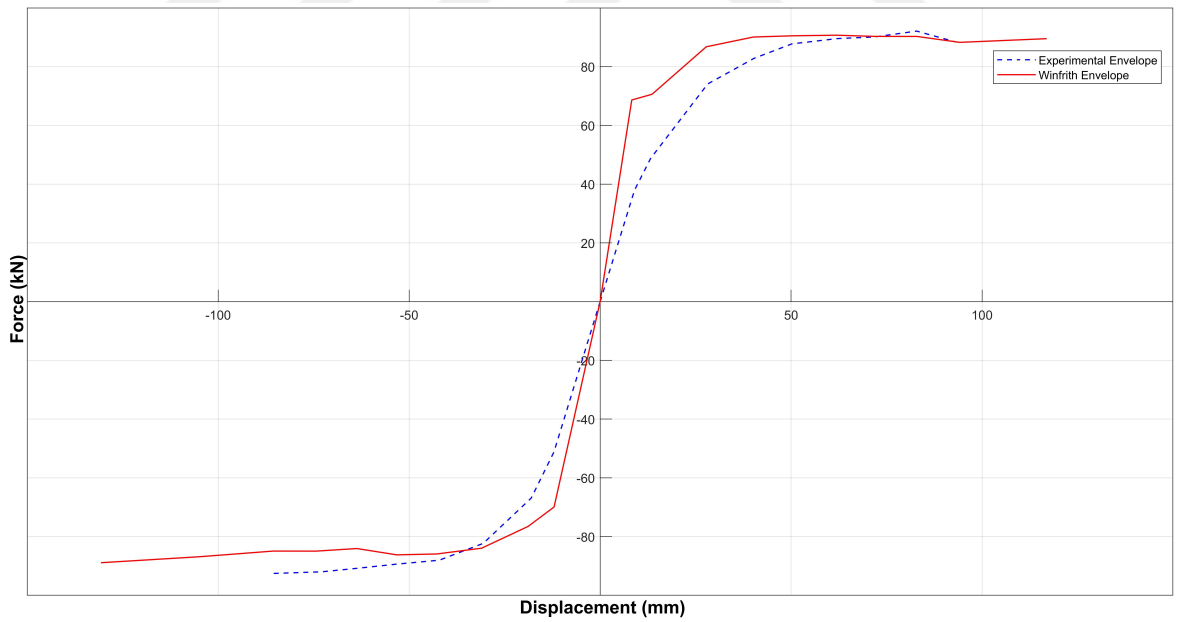

Figure 5.24. The envelope curves of the Winfrith RATE=1 model and shear critical test result.

The comparison of the model with the RATE=1 and the model with the RATE=2 for the shear critical case is demonstrated in Figure 5.25. The peak loads of the RATE=2 model are higher more than 10% on average except for the first peak load.

The RATE=2 model responded in a stiffer manner and the hysteresis curve of the model is fatter. Figure 5.26 shows the envelope curves of the Winfrith RATE=2 model and shear critical test result.

The response of the model with the RATE=0 is softer compared to the model with the RATE=1 in the first two cycles. After the second cycle, the model with the RATE=0 and RATE=1 gave similar results but the RATE=0 model showed slightly higher peak loads in the negative displacement region. The comparison of the two models was made in Figure 5.27. The RATE=0 model showed steeper unloading slopes and less pinching relative to the RATE=1 model.In Figure 5.28, the envelope curve of the Winfrith model with RATE=0 is compared with the shear critical test results.

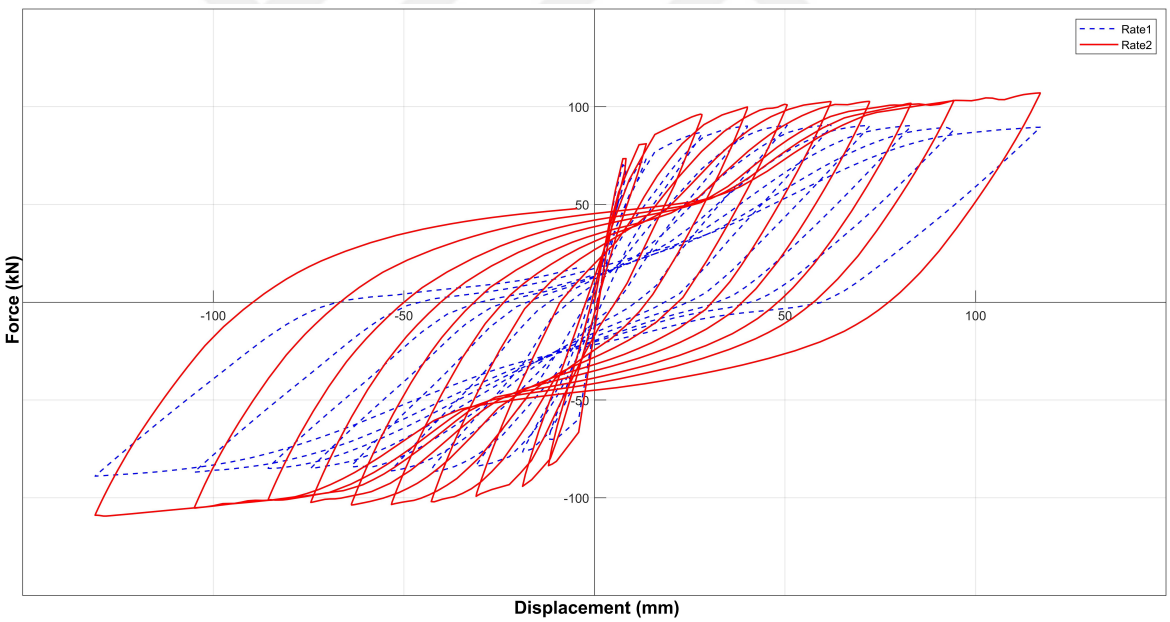

Figure 5.25. The comparison of the Winfrith models with RATE=1 and RATE=2 for the shear critical case.

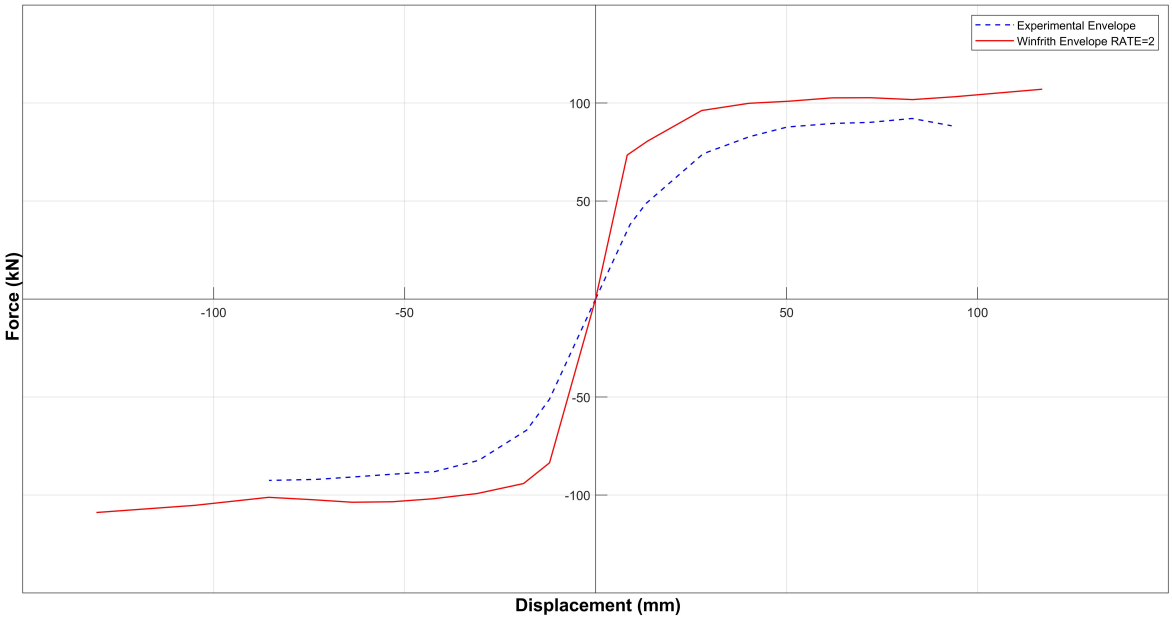

Figure 5.26. The envelope curves of the Winfrith RATE=2 model and shear critical test result.

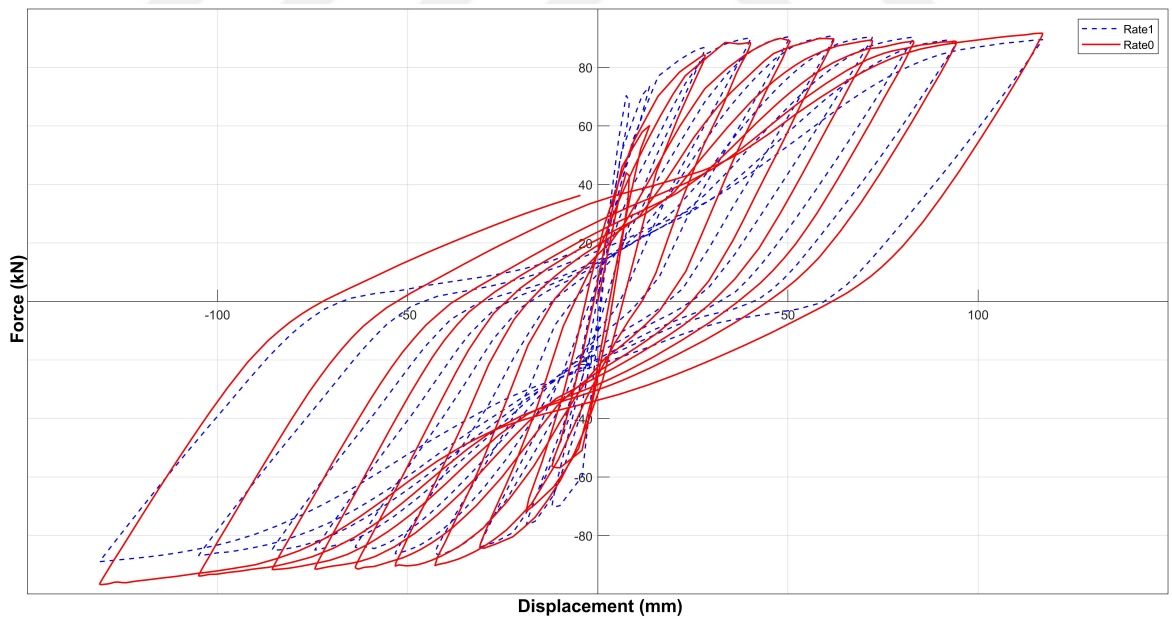

Figure 5.27. The comparison of the Winfrith models with RATE=1 and RATE=0 for the shear critical case.

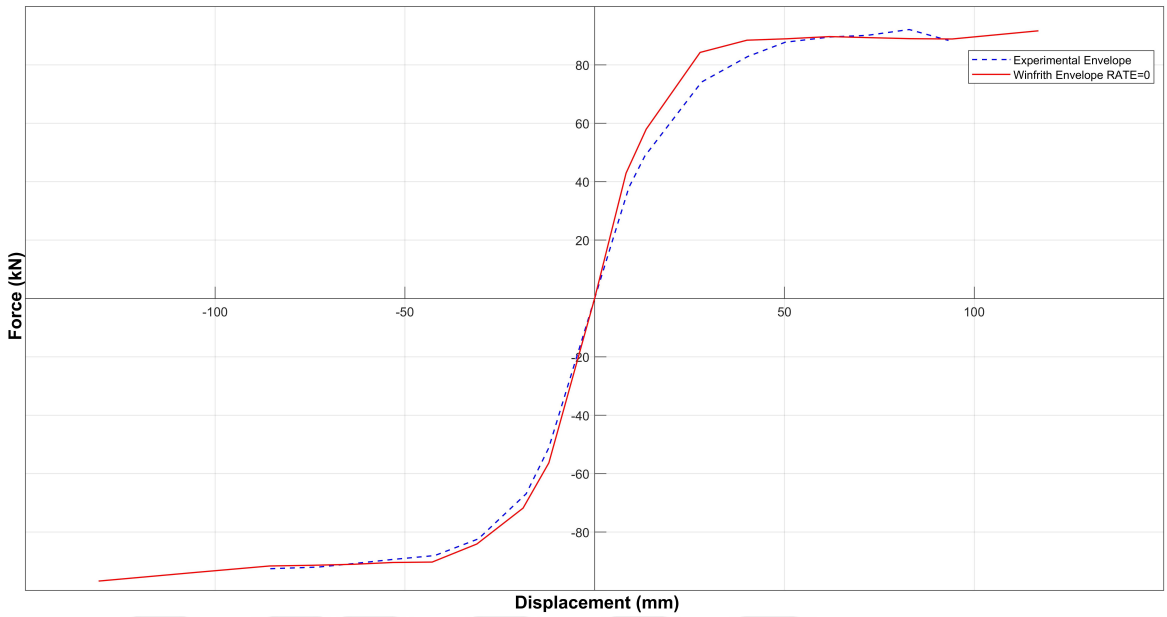

Figure 5.28. The envelope curves of the Winfrith RATE=0 model and shear critical test result.

5.2.3. MAT_159 CSCM Results

The force-displacement curves of the experimental study and the model with MAT_159 for the shear critical case were compared in Figure 5.29. The model underestimated the first peak load by about 60% but overestimated the second peak of the first cycle by 20%. In the second cycle, the model caught the peak loads. The difference between the predicted and measured peak loads for the remaining cycles are within 10%. The envelopes of the force-displacement curves are depicted in Figure 5.30. The stiffness degradation and the unloading slopes of the model are similar to the CSCM in the bending critical case. The model showed no pinching. The dissipated energy of the numerical model is higher than the experimental results.

The peak loads of the CSCM are close to the experimental results but the shape of the hysteresis curve is different as in the bending critical case. No strength loss was observed during the simulation. Lastly, the model did not fail and completed all cycles.

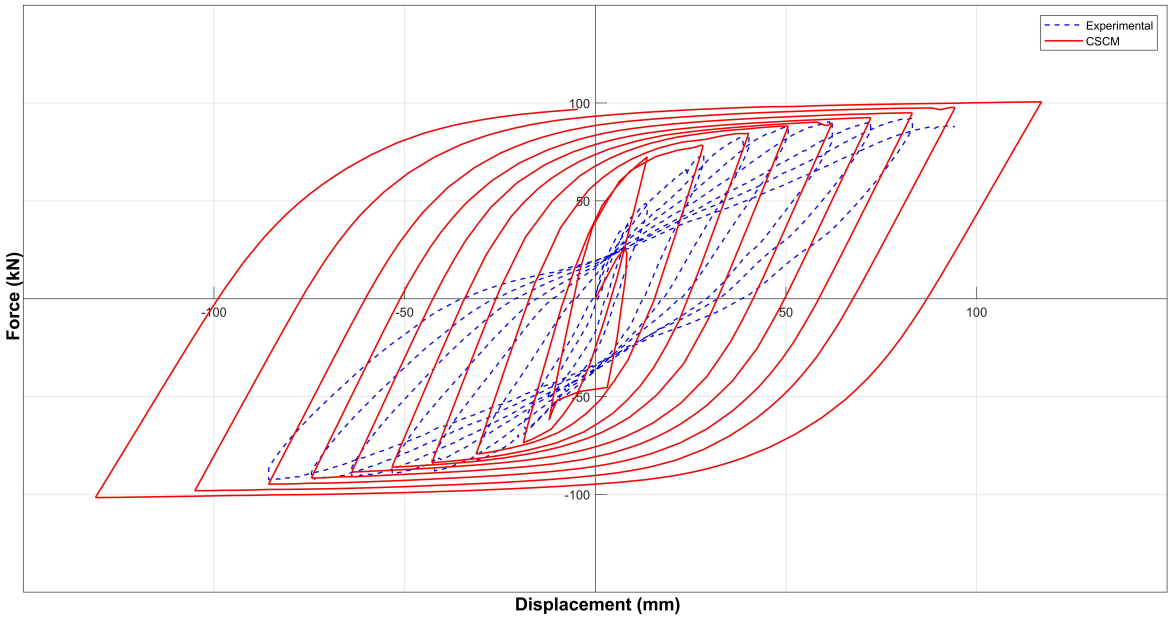

Figure 5.29. The comparison of the CSCM with shear critical test result.

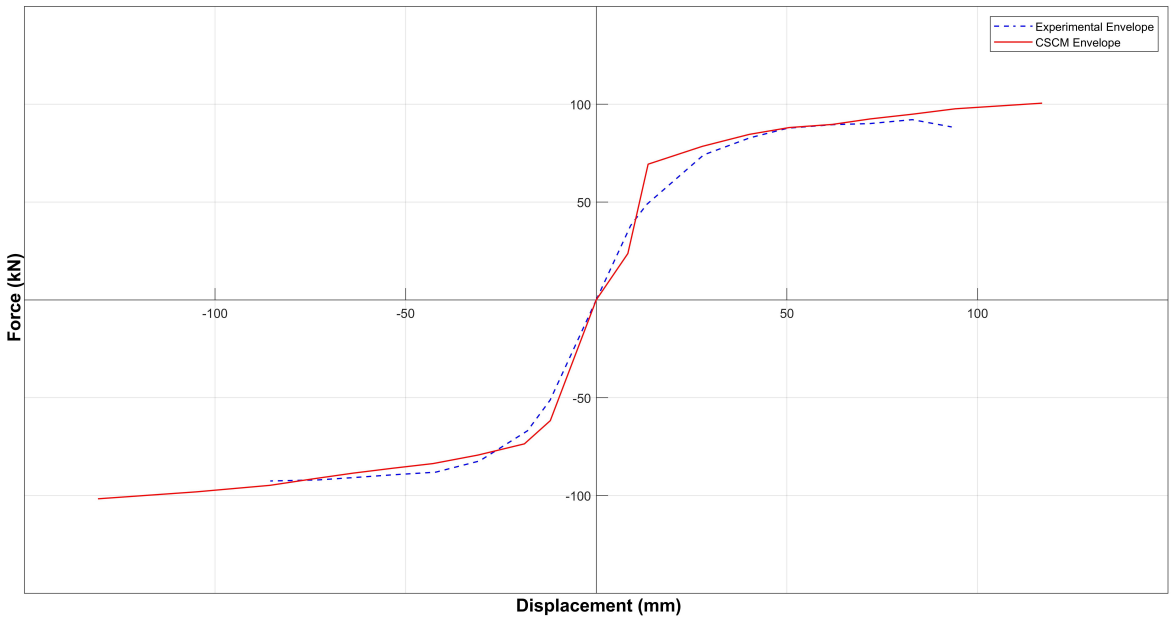

Figure 5.30. The envelope curves of the CSCM and shear critical test result.

5.2.4. MAT_272 RHT Results

The force-displacement curve of the RHT model compared with the experimental result is illustrated in Figure 5.31. The model significantly overestimated the first peak load by 128%. This trend continued in the second cycle and then, the model started to

lose strength during the second half of the second cycle. In Figure 5.32, the envelopes of the force-displacement curves are depicted.

The RHT model overestimated the peak values for the first two cycles and the stiffness degradation in these cycles was slower than the experimental results. However, the model lost strength in the third and fourth cycles and completely failed in the fourth cycle. The failed model is shown in Figure 5.33.

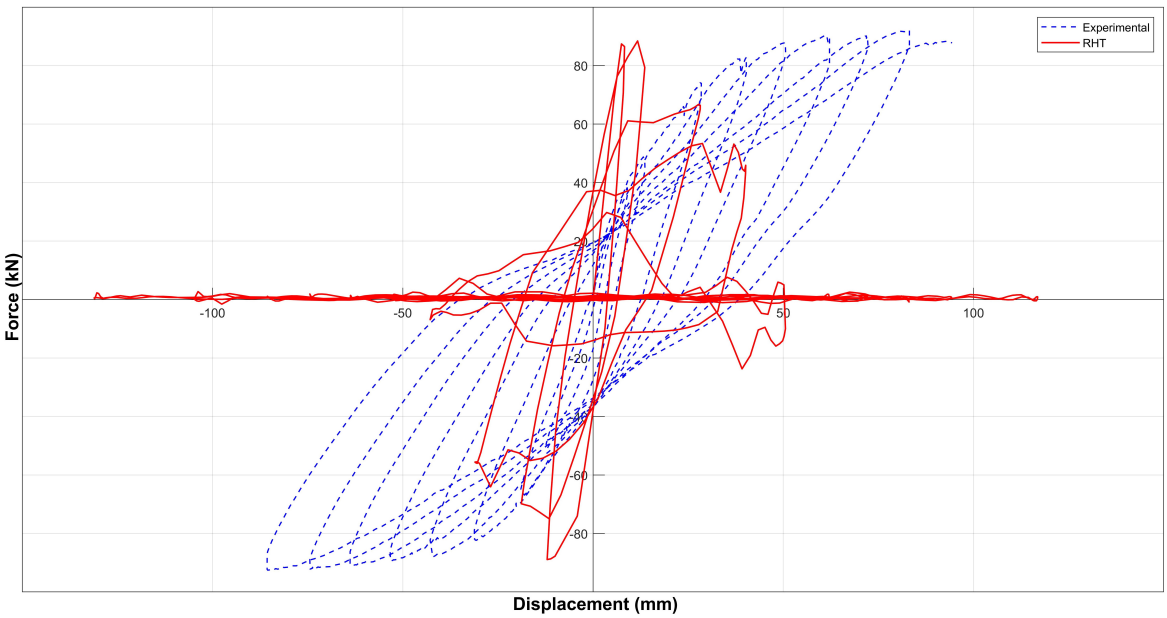

Figure 5.31. The comparison of the RHT model with shear critical test result.

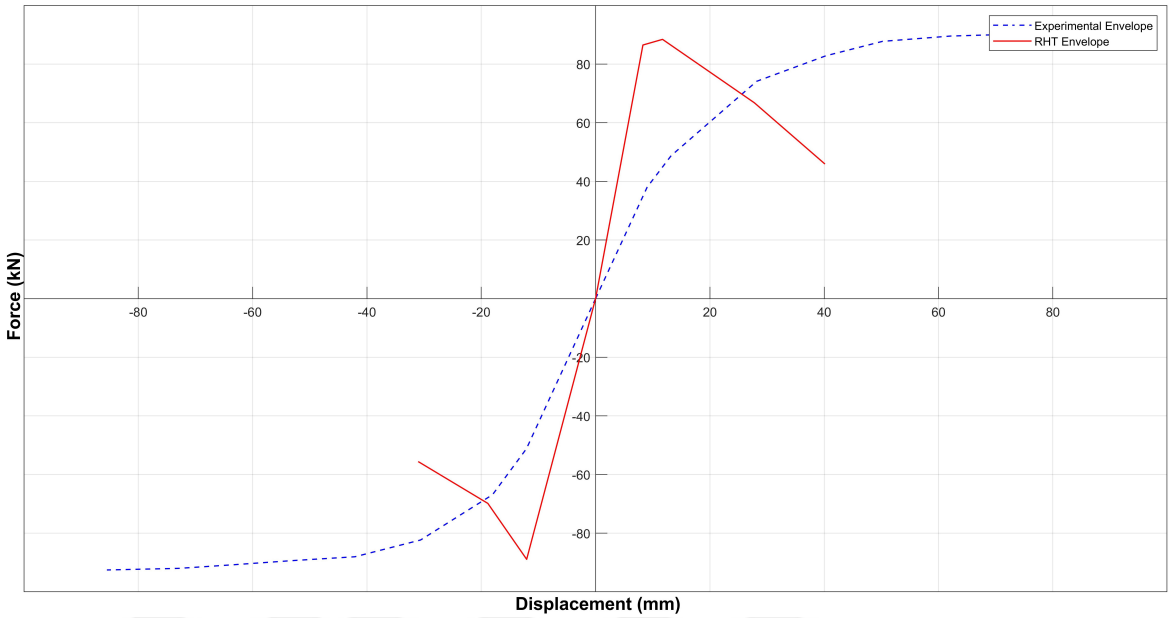

Figure 5.32. The envelope curves of the RHT model and shear critical test result.

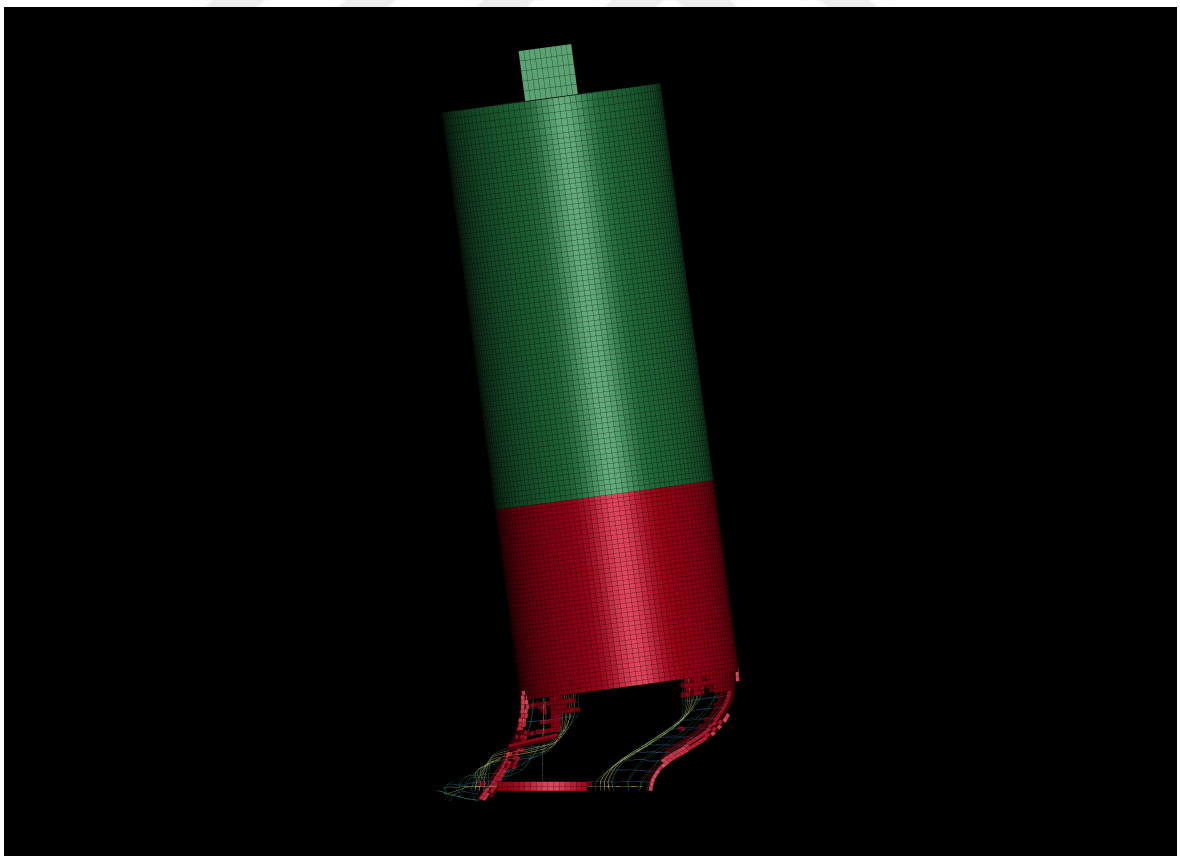

Figure 5.33. The failed RHT model for the shear critical case.

5.3. Optimum simulation parameters for Winfrith

In the light of the sensitivity analysis of the Winfrith model's input parameters, it was concluded that the models with RATE=2 gave stiffer results compared to the experimental results and it is better to use RATE=0 or the RATE=1 options for more accurate prediction of the peak loads. Table 5.1 summarizes the sensitivity analysis of the Winfrith model. In Figure 5.34 and 5.35, the force-displacement curves of the Winfrith model with RATE=0 and RATE=1 were compared with the bending critical and shear critical test results, respectively. The elastic moduli of the RATE=1 models were reduced by half to decrease the initial stiffnesses. The predictions of the two models are similar but the peak loads and the unloading slopes of the RATE=0 models are closer to the experimental results in both of the cases. Lastly, the predicted cracks larger than 0.5 mm are depicted in Figures 5.36 and Figure 5.37 for the bending critical and shear critical test results, respectively.

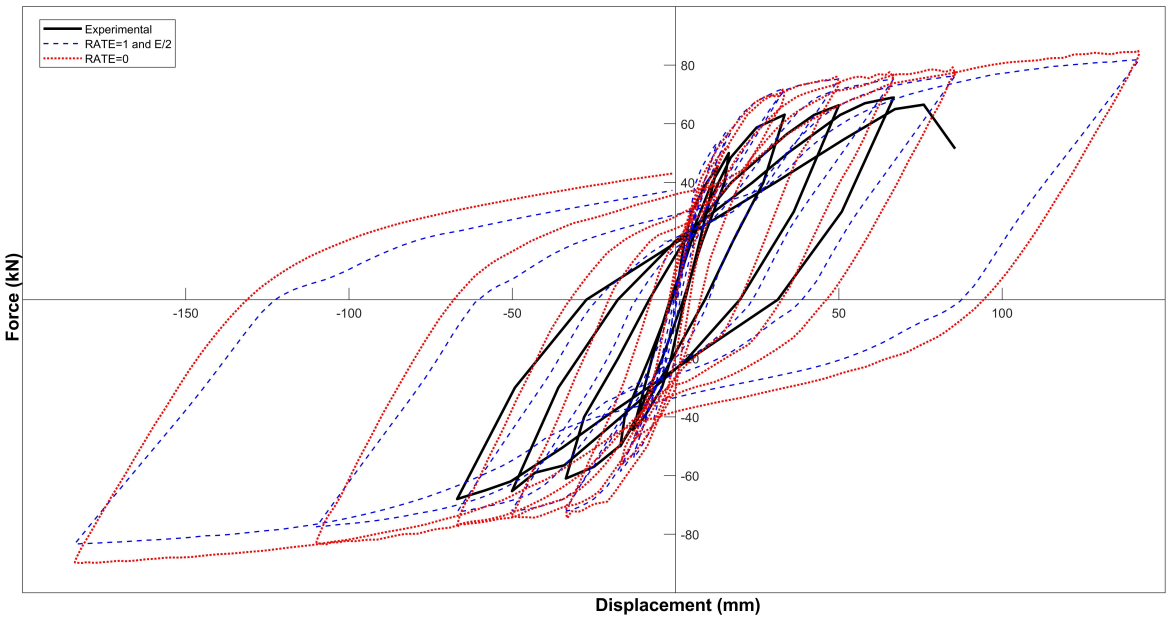

Figure 5.34. The comparison of the Winfrith model with RATE=0 and RATE=1 combined with reduced elastic modulus for the bending critical case.

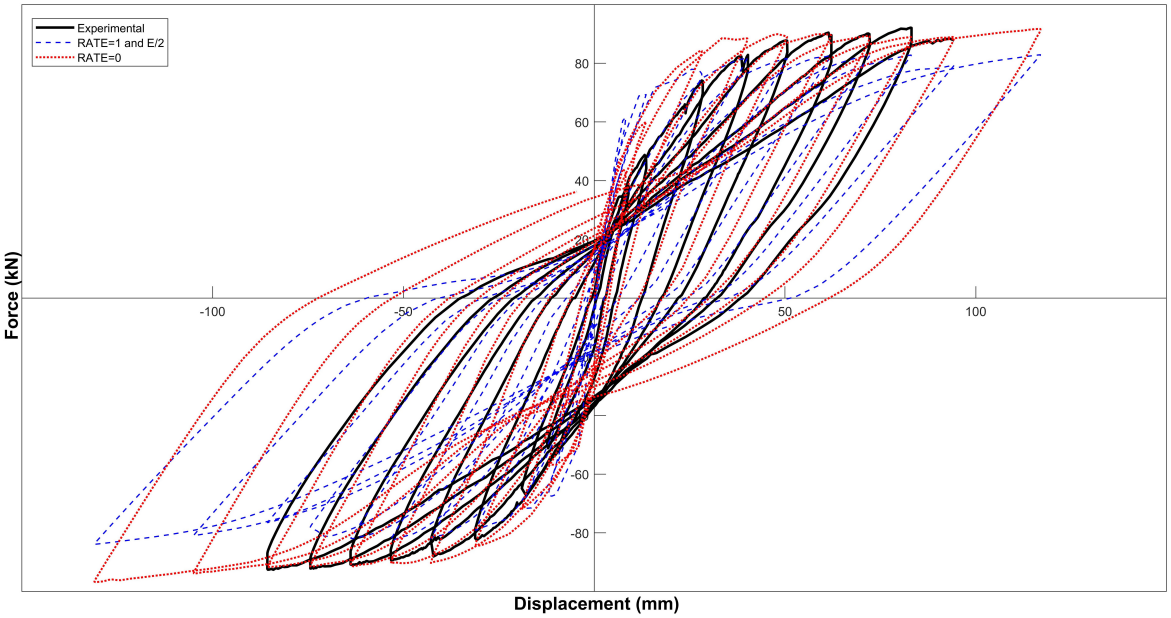

Figure 5.35. The comparison of the Winfrith model with RATE=0 and RATE=1 combined with reduced elastic modulus for the shear critical case.

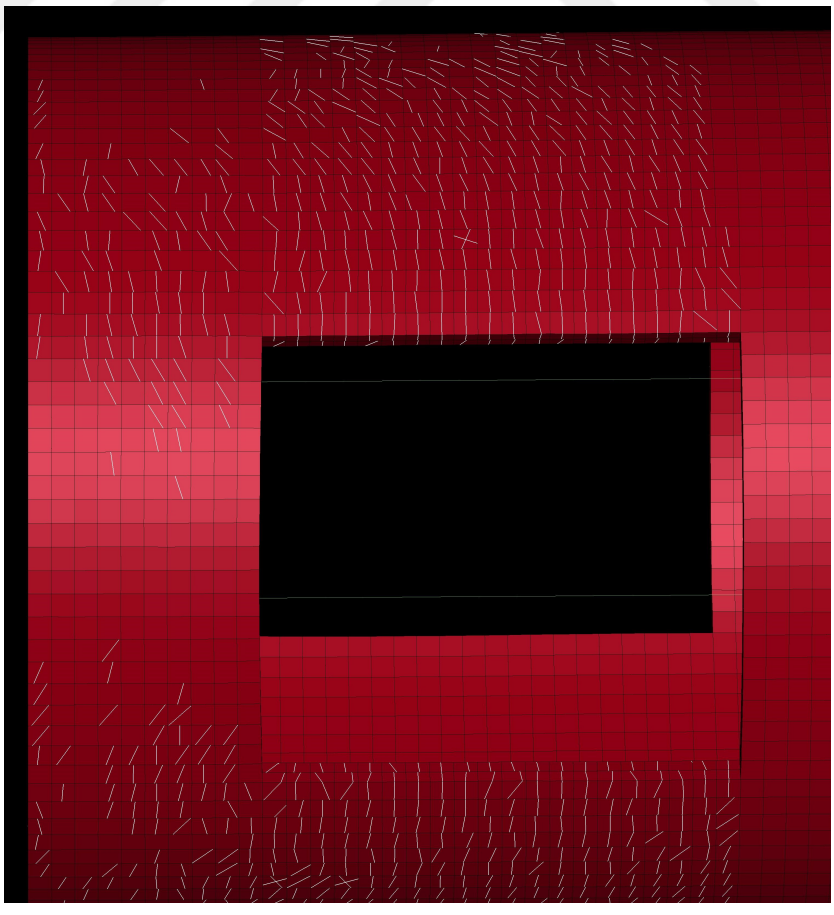

Figure 5.36. The predicted cracks for the bending critical case.

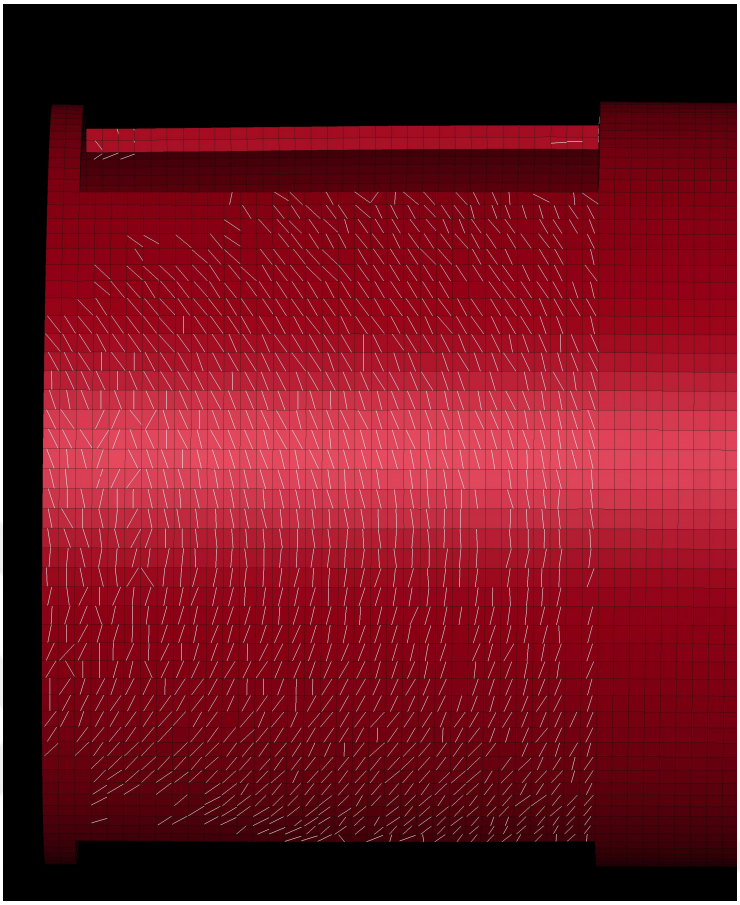

Figure 5.37. The predicted cracks for the shear critical case.

Table 5.1. The summary of sensitivity analysis of Winfrith.

Simulation Name	**RATE option**	**Figure No**	**Effect**
Winfrith RATE=1	1	5.3-5.4	Base model
Winfrith RATE=2	2	5.5-5.6	Stiffer response
Winfrith RATE=0	0	5.7-5.8	Reduced initial stiffness
Winfrith with different FE	0	5.9	Change in unloading slopes
Winfrith with different ASIZE	1	5.10	Negligible
Winfrith with different UTS	1	5.11	Initial stiffness and unlaoding slopes
Winfrith with different TM	1	5.12	Initial stiffness and unlaoding slopes
Winfrith with different UCS	1	5.13	Negligible
Winfrith with different ETAN	1	5.15	Negligible
Winfrith with different SIGY	1	5.14	Peak loads and unloading slopes

6. SUMMARY AND CONCLUSIONS

6.1. Overview

In this study, the performance of 4 different concrete material models in LS-DYNA, MAT_072R3 K&C, MAT_084 Winfrith, MAT_159 CSC, MAT_272 RHT, was evaluated to predict the cyclic behavior of reinforced concrete chimney sections. Nonlinear finite element analyses of two different RC chimney sections were carried out. The results of the numerical models were compared with the experimental results. The comparison of the force-displacement envelope curves of the models and the experimental results were made. The difference between the experimental results and the numerical models was indicated in terms of peak loads, the loading-unloading slopes, the shape of hysteresis loops, and pinching behavior.

The parameters of MAT_084, UCS, UTS, RATE, FE, TM, and ASIZE, were investigated in detail. The effects of each parameter were discussed and the peak loads, loading-unloading slopes, and pinching behavior were compared. Furthermore, the effect of the material properties of the rebar, the tangent modulus and yielding stress, was studied.

6.2. Conclusions

Based on the nonlinear finite element analyses carried out, the following conclusions can be drawn:

- The models with MAT_072R3 did not capture the overall responses in both of the cases. The model showed premature strength loss and significantly underestimated the peak loads except for the first cycle. The K&C model with a minimum number of input parameters is not recommended to simulate the cyclic behavior of RC chimneys.

- The CSCM models produced similar force-displacement envelope curves to the experimental results for the bending and shear critical cases. However, the shapes of the hysteresis curves are different compared to experimental results due to the model's inability to show pinching behavior and the steeper unloading slopes. The use of CSCM with a minimum number of input parameters is not proper to predict hysteresis curves of RC chimneys.
- The models with MAT_272 overestimated all peak values for the bending critical case but showed pinching behavior. The model failed in the same cycle as the experimental result. However, the RHT model showed poor performance in the shear critical case. The model showed early strength loss and failed prematurely in the fourth cycle. The inconsistency between the performances of the model in the bending and shear critical cases shows that the RHT model needs calibration for specific cases.
- The Winfrith model captured the overall response of both cases. The initial stiffnesses of the models are higher compared to the experimental results but this is also the case for models with different material models. A reduced elastic modulus can overcome this issue. For example, Polat and Brunea [25] used half of the actual elastic modulus in the modeling of concrete-filled sandwich steel panel walls. The models with Winfrith concrete models showed similar pinching behavior to the experimental results. However, the models did not capture the failures because of the lack of an erosion parameter.
- The Winfrith model produces more stiff results when the RATE= 2 compared to RATE=1. The RATE=0 options gave a similar result to RATE=1. The RATE=1 is a better option for modeling quasi-static loadings to minimize strain rate effects. The effects of the compressive strength and the aggregate size are negligible. The change in the elastic modulus and tensile strength have similar effects. Their effects are limited to initial stiffnesses and are negligible after the second cycle.
- The stress-strain relationship of the rebars was defined by a bilinear curve. The tangent modulus that defines the slope of the second part has a negligible effect because the rebars did not experience large strains due to the limited ductility

capacity of RC chimneys. On the other hand, the yielding stress of rebars has a major effect on the hysteresis curves. 20% change in the yielding stress causes a 10% reduction in the peak loads. The yielding stress affects also the pinching behavior. Because of these, it is important to know the yielding stress of rebars especially in the case of modeling existing structures where there is less information about the structure.

To sum up, using a proper and calibrated material model for concrete structures is important to get accurate results. More validation studies are required particularly for seismic applications.

6.3. Future Studies

Due to the limited scope of the study, future work is needed. For the evaluation of the Winfrith model, the option with strain effects turned on (RATE=0) can be investigated more. The effects of simulation time can be tested provided that the dynamics effects are limited. Additionally, an erosion criterion can be defined to model the failure of the RC pipes.

The bond between the rebars and the concrete was assumed to be perfect and was modeled with merged nodes. To evaluate this assumption, a model that includes the bond-slip relationship with CONSTRAINED_BEAM_IN_SOLID keycard can be created and compared with the present models.

Lastly, a parametric study with validated models can be conducted. In particular, the effects of opening can be studied.

REFERENCES

1. Chen, W.-F., *Plasticity in Reinforced Concrete*, J. Ross Publishing, 2007.

2. Abedini, M. and C. Zhang, "Performance Assessment of Concrete and Steel Material Models in LS-DYNA for Enhanced Numerical Simulation, A State of the Art Review", *Archives of Computational Methods in Engineering*, Vol. 28, No. 4, pp. 2921–2942, 2021.

3. Coleman, D. K., *Evaluation of Concrete Modeling in LS-DYNA for Seismic Application*, Master's Thesis, The University of Texas at Austin, 2016.

4. Wang, S., L. Yan, Q. Liang and M. Xu, "Research on RHT Constitutive Model Parameters of Fiber Reinforced Concrete Based on Experiment and Numerical Simulation", *Proceedings of the 2017 2nd International Conference on Civil, Transportation and Environmental Engineering (ICCTE 2017)*, Atlantis Press, Shenzhen, China, 2017.

5. Asgarpoor, M., A. Gharavi and S. Epackachi, "Investigation of Various Concrete Materials to Simulate Seismic Response of RC Structures", *Structures*, Vol. 29, pp. 1322–1351, 2021.

6. Epackachi, S. and A. S. Whittaker, "A Validated Numerical Model for Predicting the In-Plane Seismic Response of Lightly Reinforced, Low-Aspect Ratio Reinforced Concrete Shear Walls", *Engineering Structures*, Vol. 168, pp. 589–611, 2018.

7. Bohara, R. P., G. Tanapornraweekit and S. Tangtermsirikul, "Investigation of Concrete Material Models for Analysis of Seismic Behavior of Reinforced Concrete Under Reversed Cyclic Load", *Songklanakarin Journal of Science and Technology (SJST)*, Vol. 41, No. 4, pp. 951–958, 2019.

8. Winkelbauer, B., "Phase I Evaluation of Selected Concrete Material Models in LS-

DYNA", *Civil and Environmental Engineering Theses, Dissertations, and Student Research*, 2015.

9. Wilson, J. L., "The Cyclic Behaviour of Reinforced Concrete Chimney Sections with and without Openings", *Advances in Structural Engineering*, Vol. 12, No. 3, pp. 411–420, 2009.

10. Wilson, J. L., *Earthquake Design and Analysis of Tall Reinforced Concrete Chimneys*, Ph.D. Thesis, University of Melbourne, Parkville, Victoria, 2000.

11. Wilson, J., *Experimental Study to Investigate the Cyclic Behaviour of Reinforced Concrete Chimney Sections with Openings – Test #5*, Research Report, Dept. of Civil & Environmental Engineering, The University of Melbourne, 2003.

12. Wilson, J., *Experimental Study to Investigate the Cyclic Behaviour of Reinforced Concrete Chimney Sections with Openings – Test #6B*, Research Report, Dept. of Civil & Environmental Engineering, The University of Melbourne, Australia, 2005.

13. Malvar, L. J., J. E. Crawford, J. W. Wesevich and D. Simons, "A Plasticity Concrete Material Model for DYNA3D", *International Journal of Impact Engineering*, Vol. 19, No. 9, pp. 847–873, 1997.

14. Malvar, L. J., J. E. Crawford, J. W. Wesevich and D. Simons, "A New Concrete Material Model for DYNA3D Release II: Shear Dilation and Directional Rate Enhancements", *Defense Nuclear Agency: Alexandria, VA, USA*, 1996.

15. Wu, Y., J. E. Crawford and J. M. Magallanes, "Performance of LS-DYNA Concrete Constitutive Models", *12th International LS-DYNA Users Conference*, pp. 1–14, 2012.

16. Ottosen, N., "A Failure Criterion for Concrete", *Journal of Engineering Mechanics*, Vol. 103, pp. 527–535, 1977.

17. Murray, Y., *Users Manual for LS-DYNA Concrete Material Model 159*, Technical Report, 2007.

18. Murray, Y., A. Abu-Odeh and R. Bligh, *Evaluation of LS-DYNA Concrete Material Model 159*, Technical Report, 2007.

19. Tu, Z. and Y. Lu, "Evaluation of Typical Concrete Material Models Used in Hydrocodes for High Dynamic Response Simulations", *International Journal of Impact Engineering*, Vol. 36, No. 1, pp. 132–146, 2009.

20. "LS-DYNA Keyword User's Manual", *Livermore Technology Software Corporation (LSTC)*, Vol. 971, Volume I-III, 2012.

21. Hallquist, J. O., "LS-DYNA Theory Manual", *Livermore Software Technology Corporation*, 2006.

22. Schwer, L., "Modeling Rebar : The Forgotten Sister In Reinforced Concrete Modeling", *13th International LS-DYNA Users Conference*, 2014.

23. Du Beton, C. E.-I., "CEB-FIP model code 1990", *Design Code*, 1991.

24. Schwer, L., "The Winfrith Concrete Model: Beauty or Beast? Insights Into the Winfrith Concrete Model", *8th European LS-DYNA Users Conference*, pp. 23–24, 2011.

25. Polat, E. and M. Bruneau, "Modeling Cyclic Inelastic In-Plane Flexural Behavior of Concrete Filled Sandwich Steel Panel Walls", *Engineering Structures*, Vol. 148, pp. 63–80, 2017.

APPENDIX A: COPYRIGHTS OF FIGURES

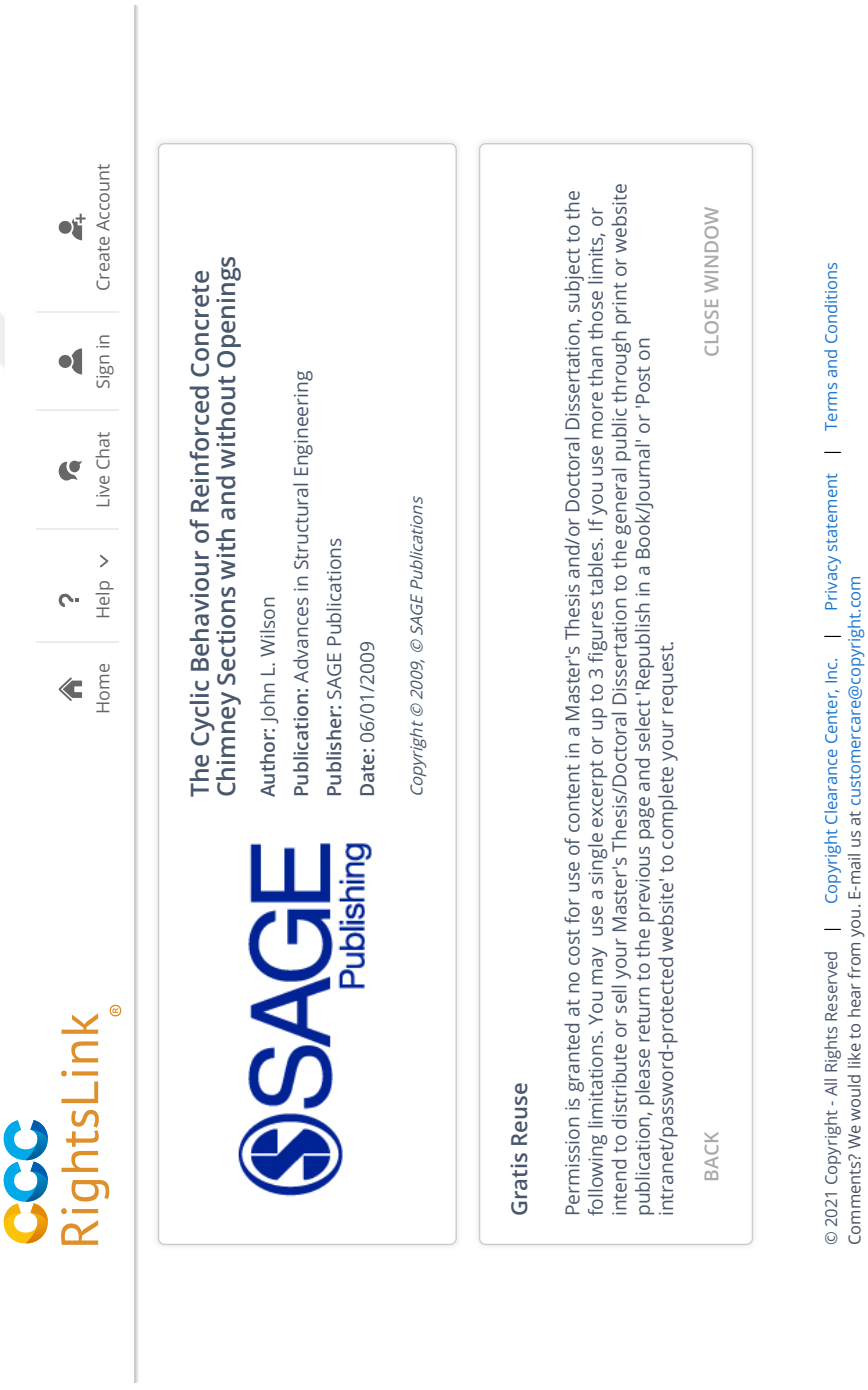

Figure A.1. Copyrights of Figure 2.1, 2.3, and 2.4.

ELSEVIER LICENSE
TERMS AND CONDITIONS

Aug 23, 2021

This Agreement between Mr. Ahmet Koç ("You") and Elsevier ("Elsevier") consists of your license details and the terms and conditions provided by Elsevier and Copyright Clearance Center.

License Number	5134961157555
License date	Aug 23, 2021
Licensed Content Publisher	Elsevier
Licensed Content Publication	International Journal of Impact Engineering
Licensed Content Title	A plasticity concrete material model for DYNA3D
Licensed Content Author	L.Javier Malvar,John E. Crawford,James W. Wesevich,Don Simons
Licensed Content Date	October–November 1997
Licensed Content Volume	19
Licensed Content Issue	9-10
Licensed Content Pages	27
Start Page	847
End Page	873

Figure A.2. Copyrights of Figure 3.1 page 1.

Type of Use	reuse in a thesis/dissertation
Portion	figures/tables/illustrations
Number of figures/tables/illustrations	1
Format	both print and electronic
Are you the author of this Elsevier article?	No
Will you be translating?	No
Title	NUMERICAL MODELING OF THE CYCLIC BEHAVIOR OF REINFORCEDCONCRETE CHIMNEY SECTIONS
Institution name	Bogazici University
Expected presentation date	Aug 2021
Portions	Figure 1

Figure A.3. Copyrights of Figure 3.1 page 2.